

*Supplementary Information to accompany*

***Ab Initio Calculations as a Quantitative Tool in the Inelastic Neutron  
Scattering Study of a Single-Molecule Magnet Analogue***

*Michele Vonci, Marcus J. Giansiracusa, Robert W. Gable, Willem Van den Heuvel, Kay Latham,  
Boujema Moubbaraki, Keith S. Murray, Dehong Yu, Richard A. Mole,\* Alessandro Soncini\* and  
Colette Boskovic\**

## Table of Contents

Experimental Section .....	S3
Synthesis .....	S3
Measurements .....	S5
Single crystal X-ray diffraction and structure solution .....	S5
Table S1.....	S6
Powder X-ray Diffraction .....	S7
Inelastic Neutron Scattering Spectroscopy .....	S7
INS Data Fitting.....	S8
Magnetic Susceptibility Measurements.....	S9
Other Measurements .....	S9
Theoretical Calculations.....	S9
Fig. S1.....	S12
Fig. S2.....	S13
Fig. S3.....	S14
Fig. S4.....	S15
Fig. S5.....	S15
Fig. S6.....	S16
Fig. S7.....	S16
Fig. S8.....	S17
Fig. S9.....	S18
Fig. S10.....	S19
Fig. S11.....	S19
Fig. S12.....	S20
Table S2.....	S21
Table S3.....	S22
Table S4.....	S23
Fig. S13.....	S24
Fig. S14.....	S25
Fig. S15.....	S26
Fig. S16.....	S26
Fig. S17.....	S27
Fig. S18.....	S27
Table S5.....	S28
Table S6.....	S29
Fig. S19.....	S30
Fig. S20.....	S31
Fig. S21.....	S32
Fig. S22.....	S33
References.....	S34

## Experimental Section

### Synthesis

All chemicals were used as purchased with no further purification.  $\text{Na}_2\text{WO}_4 \cdot 2\text{H}_2\text{O}$  (Strem, 99%),  $\text{Y}(\text{NO}_3)_3 \cdot 6\text{H}_2\text{O}$  (Strem, 99.9%),  $\text{Tb}(\text{NO}_3)_3 \cdot 5\text{H}_2\text{O}$  (Aldrich, 99.9%), glacial acetic acid (Chem-Supply, 99.7%), deuterium oxide (Sigma-Aldrich, 99.9%). The  $\text{Na}_9[\text{Ln}(\text{W}_5\text{O}_{18})_2]$  ( $\text{Ln} = \text{Tb}$  and  $\text{Y}$ ) compounds were synthesised by modification of literature methods.<sup>1</sup> Samples with deuterated hydrate molecules for INS were synthesised and handled under nitrogen using standard Schlenk and glove-box techniques.

**$\text{Na}_9[\text{Tb}(\text{W}_5\text{O}_{18})_2] \cdot x\text{H}_2\text{O}$  (Tb).** Solid  $\text{Na}_2\text{WO}_4 \cdot 2\text{H}_2\text{O}$  (14.84 g, 45.00 mmol) was dissolved in water (30 ml) and heated to 90° C. The pH was then adjusted to 7.2 with glacial acetic acid, while maintaining the tungstate solution at constant temperature. A solution of  $\text{Tb}(\text{NO}_3)_3 \cdot 5\text{H}_2\text{O}$  (1.958 g, 4.500 mmol) in hot water (4 ml), was added dropwise to the tungstate solution with vigorous stirring, affording a fine precipitate. After the addition was complete, the mixture was stirred for a further 5 minutes and then cooled at room temperature. The resulting fine precipitate was removed by filtration and the filtrate was stored at 5 °C for 24 hours. The resulting colourless crystalline product (13.1 g, 3.8 mmol, yield 85 %) was recrystallised from hot water, giving colourless crystals with a mixture of blade (**Tb-a**) and distorted hexagonal prismatic (**Tb-b**) shapes after 24 hours. Selected IR data (KBr,  $\text{cm}^{-1}$ ): 944 (m), 844 (s), 782 (m), 704 (s), 583 (w), 542 (m), 490 (w), 420 (s). It was possible to isolate a pure sample of **Tb-a** by slow recrystallization from  $\text{H}_2\text{O}$  at room temperature, whereas the formation of **Tb-b** was favored by recrystallization from the minimum amount of hot  $\text{H}_2\text{O}$  followed by cooling at 5°. Phase **Tb-a** is stable in contact with mother liquor and upon drying, although it loses crystallinity upon grinding. In the presence of mother liquor, phase **Tb-b** is metastable and slowly converts into **Tb-a**, while following isolation and drying it is deliquescent.

**Na<sub>9</sub>[Tb(W<sub>5</sub>O<sub>18</sub>)<sub>2</sub>]·20D<sub>2</sub>O (Tb<sup>D</sup>).** A sample of **Tb** (3-4 g) was heated at 150 °C under reduced pressure (100 µmHg) for 6 h. The resulting amorphous powder was recrystallised from the minimum amount of D<sub>2</sub>O under an atmosphere of dry nitrogen. The mixture of colourless blade-shaped (**Tb-a<sup>D</sup>**) and distorted hexagonal prismatic-shaped (**Tb-b<sup>D</sup>**) crystals that were obtained after 24 h were filtered dried and stored under nitrogen. The deuteration was checked by ATR-IR through the diagnostic peaks of DHO and D<sub>2</sub>O bending modes around 1440 and 1210 cm<sup>-1</sup> respectively (Fig. S1). Selected IR data (ATR-IR, cm<sup>-1</sup>): 1438 (w), 1209 (w), 967 (m), 922 (s), 830 (s), 776 (s), 699 (s), 582 (w), 540 (w), 482 (m), 413 (s). Elemental analysis for Na<sub>9</sub>[Tb(W<sub>5</sub>O<sub>18</sub>)<sub>2</sub>]·20D<sub>2</sub>O, D<sub>40</sub>Na<sub>9</sub>O<sub>56</sub>TbW<sub>10</sub>, calcd (found): D 2.52 (2.90), Tb 5.0 (4.6), Na 6.5 (6.6), W 58 (55.0). Thermogravimetric analysis confirmed the degree of hydration. A pure sample of **Tb-a<sup>D</sup>** was obtained as per the non-deuterated sample.

**Na<sub>9</sub>[Y(W<sub>5</sub>O<sub>18</sub>)<sub>2</sub>]·xH<sub>2</sub>O (Y).** Synthesised as per **Tb** using Y(NO<sub>3</sub>)<sub>3</sub>·6H<sub>2</sub>O. The sample appears to be predominantly phase a. Selected IR data (KBr, cm<sup>-1</sup>): 938 (m), 844 (s), 777 (s), 710 (s), 544 (w), 492 (w), 427 (s), 414 (s).

**Na<sub>9</sub>[Y(W<sub>5</sub>O<sub>18</sub>)<sub>2</sub>]·20D<sub>2</sub>O (Y<sup>D</sup>).** Synthesised as per **Tb<sup>D</sup>**. Selected IR data (ATR-IR, cm<sup>-1</sup>): 1435 (w), 1209 (w), 968 (m), 941 (m), 924 (s), 910 (m), 836 (s), 773 (s), 698 (s), 585 (w), 548 (w), 483 (w), 415 (s). Elemental analysis for Na<sub>9</sub>[Y(W<sub>5</sub>O<sub>18</sub>)<sub>2</sub>]·20D<sub>2</sub>O, D<sub>40</sub>Na<sub>9</sub>O<sub>56</sub>W<sub>10</sub>Y, calcd (found): H 2.57 (2.85), Y 2.9 (2.7), Na 6.65 (7.0), W 59 (53).

## Measurements

### Single Crystal X-ray Diffraction and Structure Solution

Diffraction measurements (Table S1) were performed on an Agilent Technologies SuperNova diffractometer using CuK $\alpha$  radiation ( $\lambda = 1.54184 \text{ \AA}$ ) at 130 K. Gaussian absorption correction was applied for all compounds. The structures were solved by direct methods approach using SHELXT 2014 structure solution program and refined through full-matrix least-squares techniques on  $F^2$  by using the SHELXL 2014 crystallographic software package. For all structures all atoms in the  $[\text{Ln}(\text{W}_5\text{O}_{18})_2]^{9-}$  unit were refined anisotropically. For **Y** and **Tb-a** it was possible to also refine the sodium cations and the oxygen atoms from the water molecule anisotropically, whereas in **Tb-b** these were refined isotropically. The positional disorder of the sodium cations and water molecules in **Tb-b** was modelled splitting atoms, using SUMP restraints and fixing the chemical occupancy of the oxygen atoms of the solvent. For all the three structures the H-atom parameters were not defined. Further details on the crystal structure investigations may be obtained from the Fachinformationszentrum Karlsruhe, 76344 Eggenstein-Leopoldshafen, Germany (fax: (+49)7247-808-666; e-mail: [crysdata@fiz-karlsruhe.de](mailto:crysdata@fiz-karlsruhe.de)), on quoting the depository numbers ICSD-429951, -429952, and -429953).

**Table S1.** Single Crystal X-ray Diffraction Data and Refinement Parameters for **Tb-a**, **Tb-b** and **Y**

	<b>Tb-a</b>	<b>Tb-b</b>	<b>Y</b>
Empirical formula	$\text{Na}_9\text{O}_{71}\text{TbW}_{10}\text{H}_{70}$	$\text{Na}_9\text{O}_{72}\text{TbW}_{10}\text{H}_{72}$	$\text{YNa}_9\text{O}_{71}\text{W}_{10}\text{H}_{70}$
Formula weight	3410.89	3428.90	3340.88
Temperature / K	130.0(1)	131.1(1)	130.0(1)
Crystal system	triclinic	triclinic	triclinic
Space group	<i>P</i> -1	<i>P</i> -1	<i>P</i> -1
<i>a</i> / Å	12.7251(4)	12.8949(5)	12.7357(5)
<i>b</i> / Å	13.0624(4)	13.1098(5)	13.0732(4)
<i>c</i> / Å	20.4974(7)	20.9057(7)	20.4565(8)
$\alpha$ / °	82.857(3)	76.956(3)	82.865(3)
$\beta$ / °	74.521(3)	83.954(3)	74.492(4)
$\gamma$ / °	88.927(3)	77.348(3)	88.859(3)
Volume / Å <sup>3</sup>	3257.65(19)	3353.5(2)	3256.2(2)
<i>Z</i>	2	2	2
$\rho_{\text{calc}}$ / gcm <sup>3</sup>	3.477	3.396	3.407
$\mu$ / mm <sup>-1</sup>	38.720	37.561	34.502
<i>F</i> (000)	3084.0	3104.0	3032.0
Crystal size / mm <sup>3</sup>	0.1723 × 0.1367 × 0.0300	0.1477 × 0.0402 × 0.0344	0.1586 × 0.0193 × 0.0127
Radiation	CuK $\alpha$ ( $\lambda$ = 1.54184)	CuK $\alpha$ ( $\lambda$ = 1.54184)	CuK $\alpha$ ( $\lambda$ = 1.54184)
2θ range for data collection / °	6.82 to 143.432	7.038 to 142.998	6.814 to 148.164
Index ranges	-15 ≤ <i>h</i> ≤ 15, -16 ≤ <i>k</i> ≤ 16, -24 ≤ <i>l</i> ≤ 25	-15 ≤ <i>h</i> ≤ 15, -15 ≤ <i>k</i> ≤ 16, -25 ≤ <i>l</i> ≤ 25	-13 ≤ <i>h</i> ≤ 15, -16 ≤ <i>k</i> ≤ 16, -24 ≤ <i>l</i> ≤ 25
Reflections collected	22002	22609	23776
Independent reflections	12145 [ $R_{\text{int}} = 0.0454$ , $R_{\text{sigma}} = 0.0425$ ]	12708 [ $R_{\text{int}} = 0.0364$ , $R_{\text{sigma}} = 0.0615$ ]	12808 [ $R_{\text{int}} = 0.0437$ , $R_{\text{sigma}} = 0.0747$ ]
Data / restraints / parameters	12145/0/820	12708/19/848	12808/0/820
Goodness-of-fit on $F^2$	1.085	1.052	1.017
Final <i>R</i> indexes [ $I \geq 2\sigma(I)$ ]	$R_1 = 0.0476$ , $wR_2 = 0.1329$	$R_1 = 0.0353$ , $wR_2 = 0.0863$	$R_1 = 0.0354$ , $wR_2 = 0.0822$
Final <i>R</i> indexes [all data]	$R_1 = 0.0501$ , $wR_2 = 0.1364$	$R_1 = 0.0439$ , $wR_2 = 0.0912$	$R_1 = 0.0446$ , $wR_2 = 0.0879$
Largest diff. peak / hole / e Å <sup>-3</sup>	2.56/-3.03	4.49/-2.61	1.44/-2.39

## Powder X-ray Diffraction

Data were acquired on a Bruker D4 ENDEAVOR X-ray diffractometer, fitted with a Lynx-Eye Position Sensitive Detector, and using a copper tube source ( $\text{CuK}\alpha$ ,  $\lambda = 1.5406 \text{ \AA}$ ), operated at 40 kV and 35 mA. Data was collected with 5-40 degree 2 theta angle range with a 0.02 degree step size and a 2 s per step dwell time. The loss of crystallinity of both phases and metastability of **Tb-b** makes it difficult to obtain finely ground microcrystalline samples, especially of pure **Tb-b**. Thus powder X-ray diffraction data were collected on coarsely ground, air-dried samples under ambient conditions, which are likely to exhibit some preferential orientation of the crystallites. This tends to alter the relative intensities of the peaks in the experimental patterns compared to those simulated from the single crystal X-ray diffraction data. As a result, although the powder diffraction data are consistent with the presence of two phases in the mixed **Tb<sup>D</sup>** sample, it is not possible to quantitatively establish the relative proportions of the two phases on the basis of these data.

## Inelastic Neutron Scattering Spectroscopy

Coarsely ground, crystalline samples (1.5-2.5 g) of **Tb<sup>D</sup>**, **Tb-a<sup>D</sup>**, **Y<sup>D</sup>** were analysed in a 1 mm annular Al can. The background due to the empty sample can was subtracted and the data normalised to a vanadium standard. All data manipulations were carried out using the large array manipulation program LAMP.<sup>2,3</sup> The sample was cooled using a displex type cryostat and data collected at 5, 10, 15, 30, and 40 K for **Tb<sup>D</sup>** and at 5, 15 and 40 K for **Tb-a<sup>D</sup>**. The data of **Y<sup>D</sup>** were collected at 10 and 50 K. By opportune phasing of the choppers each sample was analysed with two different neutron wavelength (4.74 and 2.37  $\text{\AA}$ ) then offering complementary information. Better resolution and better access to the neutron energy gain side of the spectrum, but a narrower overall energy transfer range (3.64 meV) is available at the higher neutron wavelength, while the lower wavelength gives access to a broader

energy transfer range (14.6 meV), allowing the observation of otherwise inaccessible transitions on the energy loss side of the spectrum, but with lower resolution.

## INS Data Fitting

A minimal set of Extended Stevens Operators were used to set-up a simplified CF Hamiltonian, consisting of only three (**Tb-a**) or two (**Tb-b**) CFPs. The selection of the CFPs incorporated in this simple model Hamiltonian, and their correlation with the actual geometrical structure of the molecule, was solely guided by the *ab initio* results and the symmetry arguments given in the text. The experimental INS data for **Tb-a** and **Tb-b** were fit to the simplified CF Hamiltonian, optimising the selected three (**Tb-a**) or two (**Tb-b**)  $B_k^q$  parameters (Table 2) of:

$$\sum_{k=2,4,6} \sum_{q=-k}^k B_k^q \hat{O}_k^q$$

where  $\hat{O}_k^q$  are the extended Stevens operators.<sup>4</sup>

The two sets of CF field parameters were optimised using the *simannfit* fitting module of the MCPHASE modelling suite,<sup>5</sup> using the values of the CF parameters determined by *ab initio* calculations as a first guess. Many other sets of initial CF parameters were also employed and the fitting program either converged to the same solution or did not converge to any solution. The fitting strategy uses a simulated annealing algorithm to iteratively minimise the standard deviation between the simulated and the experimental INS spectra.<sup>6</sup> During the iterative fitting procedure the spectrum of the theoretical INS transition probabilities is convoluted with Gaussian functions of appropriate FWHM (870 μeV for  $\lambda = 2.37$  Å and 250 μeV for  $\lambda = 4.74$  Å) to generate the simulated INS spectrum to be compared to the experimental one. The experimental data fitted were peaks Ia, IIa, IIIa, Iva and Va of **Tb-a** at 40 K and peaks Ib and IIb of **Tb** at 30 K. The 0.3 meV peak was present in all data at all temperatures and assigned as spurious.

## Magnetic Susceptibility Measurements

Variable temperature magnetic susceptibility measurements were performed with a Quantum Design MPMS-5 susceptometer, equipped with a 5 T magnet. Data were collected on powdered, dry crystals in a gelatin capsule. The diamagnetic susceptibility was measured for **Y** and found to be very similar to the diamagnetic correction calculated from Pascal's constants, which was employed to correct the magnetic susceptibility measured for **Tb**.

## Other Measurements

Elemental analyses were performed by the Campbell Microanalytical Laboratory, University of Otago, New Zealand. Thermogravimetric analyses were performed on a Mettler Toledo thermal analyzer. Infrared spectra (KBr disk or ATR) were recorded on a Bruker Tensor 27 FTIR spectrometer.

## Theoretical Calculations

The *ab initio* calculations were carried out using the commercial Molcas 8.0 software package.<sup>[7–9]</sup> The typical timeframe for a full calculation was 72–96 h.

The structural inputs of calculations for **Tb-a** and **Tb-b** were the Cartesian coordinates of the isolated  $[\text{Tb}(\text{W}_5\text{O}_{18})_2]^{9-}$  anion obtained from high quality single crystal X-ray diffraction data at 130 K, with no addition of counterions to balance the charge (table S6a). The point symmetry for the isolated  $[\text{Tb}(\text{W}_5\text{O}_{18})_2]^{9-}$  anion used in the calculations is C<sub>1</sub>. The z axis of the Cartesian reference system was chosen to incorporate atoms Tb1 and W1 for **Tb-a** and W1 and W10 for **Tb-b**. The *ab initio* calculations do not take into account the electrostatic potential arising from the crystal, as they are done on the isolated C<sub>1</sub> symmetry anion. From a computational point of view, the presence of the {W<sub>5</sub>O<sub>18</sub>} ligands makes any attempt to use a full basis to describe the heavy W atoms extremely demanding. In order to reduce the computational load all W atoms were represented with an *ab initio*

Model Potential (W.ECP.Casarrubios.13s10p9d5f.3s3p4d2f.12e-CG-AIMP), using the basis set contraction suggested by Molcas.<sup>10,11</sup> For other elements ANO-RCC basis sets were employed, with a TZP quality basis set for Tb and DZP quality basis set for O.

The well-established procedure that provides the full *ab initio* electrostatic and strongly spin-orbit coupled eigenvalues and eigenvectors, including the full treatment of static correlation effects via complete-active space methods, involves the use of different modules of Molcas 8.0 (SEWARD + RASSCF + RASSI). In the computation of the bi-electronic integrals performed by the *SEWARD* module the Cholesky decomposition with a threshold of  $10^{-8}$  was used in order to save disk space.

The spin-only wavefunctions corresponding to the spin multiplicity of 7, 5, 3, and 1 were optimised using the Complete Active Space Self-Consistent Field (CASSCF) method supplied by the module RASSCF, (Restricted Active Space Self Consistent Field) with the active space set as the 8 electrons of Tb(III) in the 4f orbitals.<sup>12</sup> The module *RASSI* (Restricted Active Space State Interaction) was used to introduce the spin–orbit coupling with the restricted active space state interaction method.<sup>13</sup> A selected number of different spin states (149) were allowed to interact in the RASSI module, namely 7 septets (out of 7), 84 quintets (out of 140) and 58 (out of 588) triplets. None of the 490 singlets were included in the calculations because of their high energy. The static magnetic properties, the components of the lowest lying *ab initio* wavefunctions projected onto a  $(2J+1)$ -dimensional pseudo-spin basis set (Table S3 and S4), and the crystal field parameters (Table S5) were finally calculated from the CASSCF/RASSI results employing a rigorous, well-established and widely used projection technique implemented in the SINGLE\_ANISO module of Molcas 8.0.<sup>14</sup>

In the SINGLE\_ANISO computation the reference frame used for the quantisation of the total angular momentum basis when projecting the full *ab initio* wavefunctions on to the effective spin-orbit ground multiplet ( $J = 6$ ) of the Tb(III) ion corresponds to the three

principal magnetic axes of the calculated g-tensor for the lowest energy quasi-degenerate doublet (first excited doublet) with the origin of the reference system lying on the Tb(III) ion (Table S6b and Figure S19). The choice of the quantisation axis along the z component of the g tensor allows the projections of the lowest lying CASSCF/RASSI wavefunctions onto the  $(2J+1)$ -dimensional basis to have almost pure  $\pm M_J$  components (Table S3 and S4). It turns out that the anisotropy axis, as determined from the g-tensor of the first excited pseudo doublet, is approximately coincident with the pseudo  $C_4$  axis of the molecule (Table S6b).

The matrix elements of the all-electron spin and angular momentum operators between low-lying optimised ab-initio CASSF/RASSI wavefunctions corresponding to the crystal field levels were used to calculate transition probabilities (i.e. INS peak intensities) in the reported theoretical INS spectra.

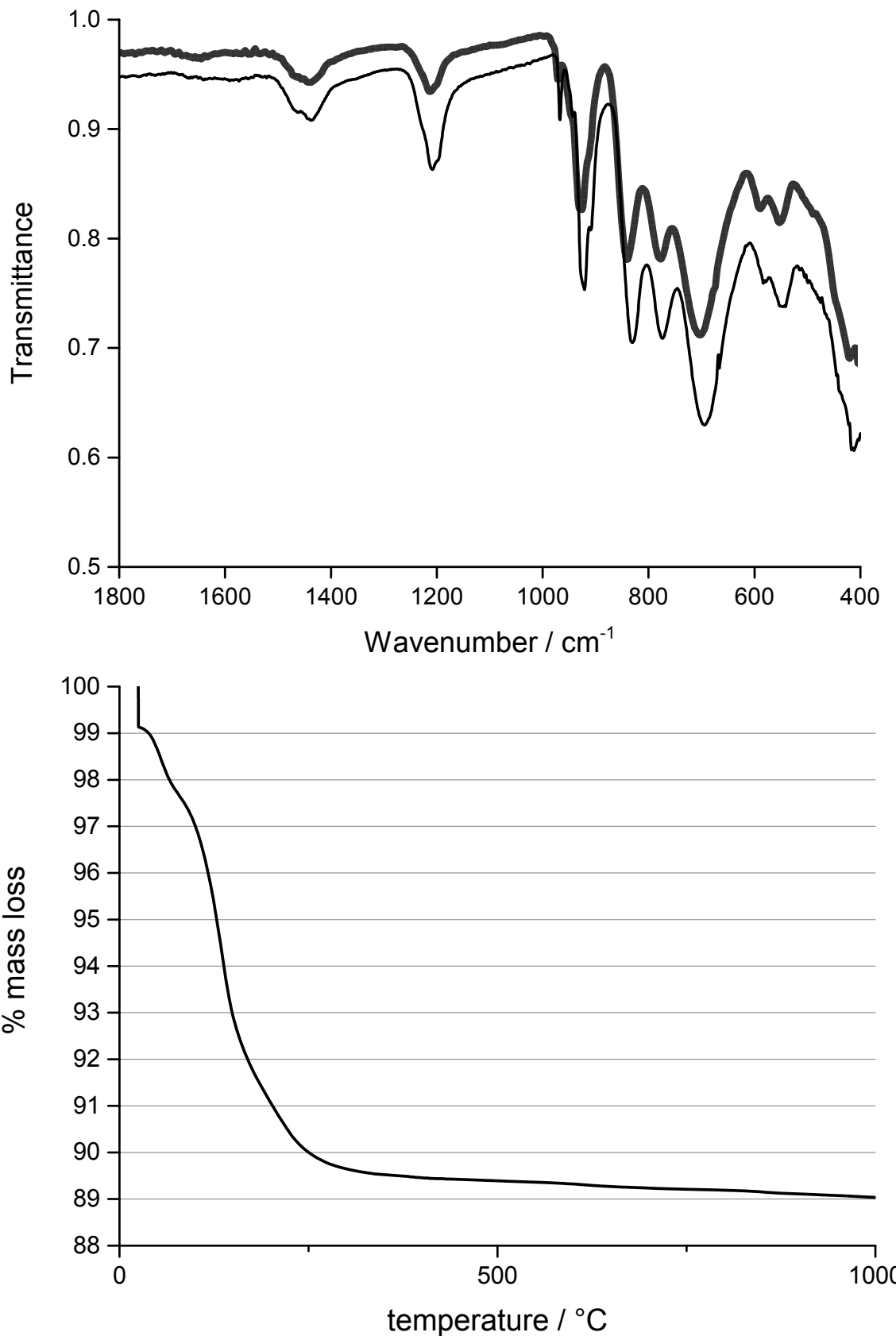


**Fig. S1** Top: Measured ATR-IR spectra for  $\text{Tb}^{\text{D}}$  (thin line) and  $\text{Y}^{\text{D}}$  (thick line). Bottom: Thermogravimetric analysis data for  $\text{Tb}^{\text{D}}$

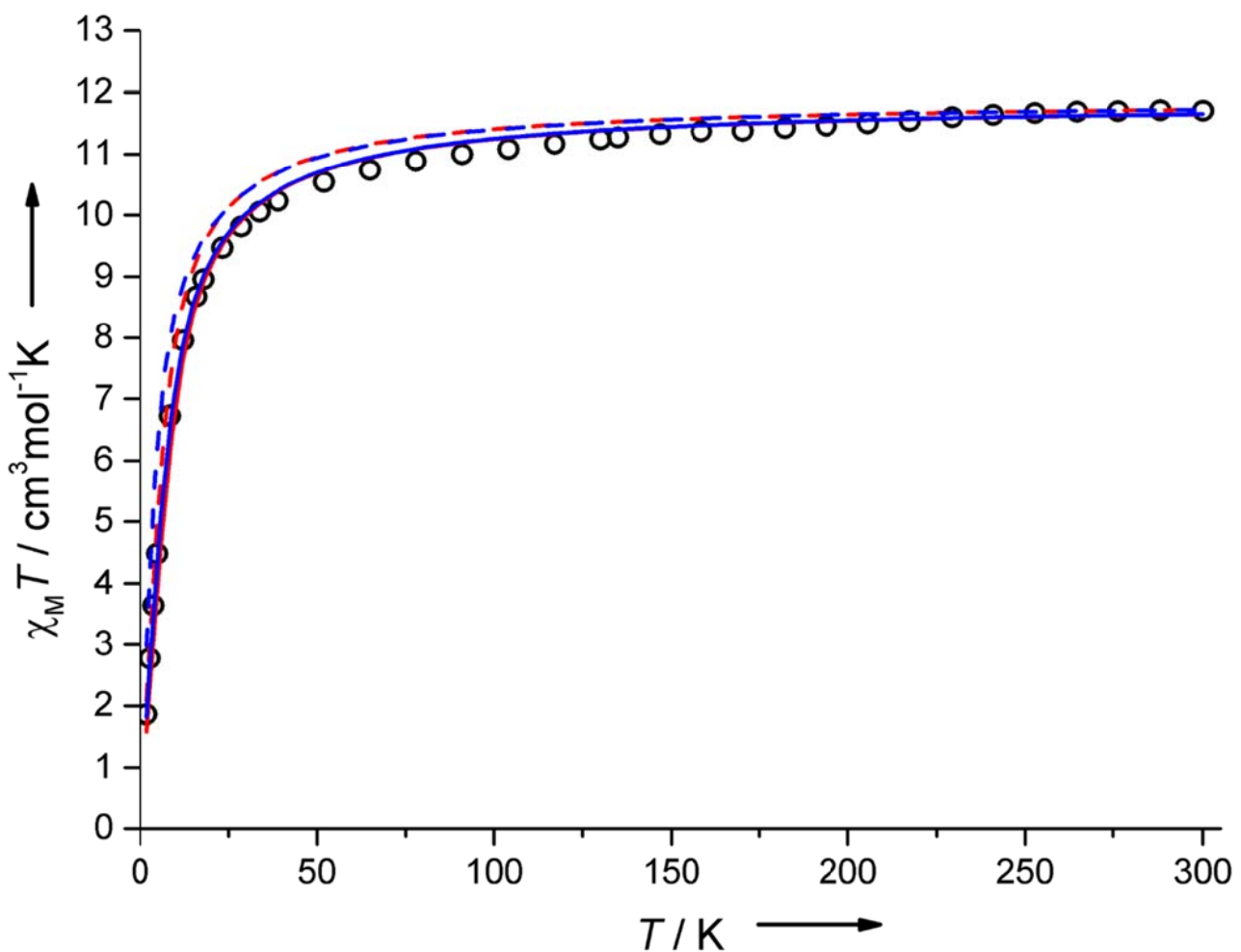


**Fig. S2**  $T$  dependence of the  $\chi_M T$  product in the 2–300 K range for **Tb-a**. Solid lines: *ab initio* simulation for **Tb-a** (red) and **Tb-b** (blue). Dashed lines: simulations for **Tb-a** (red) and **Tb-b** (blue) using the sets of optimised crystal field parameters as described in the main text.

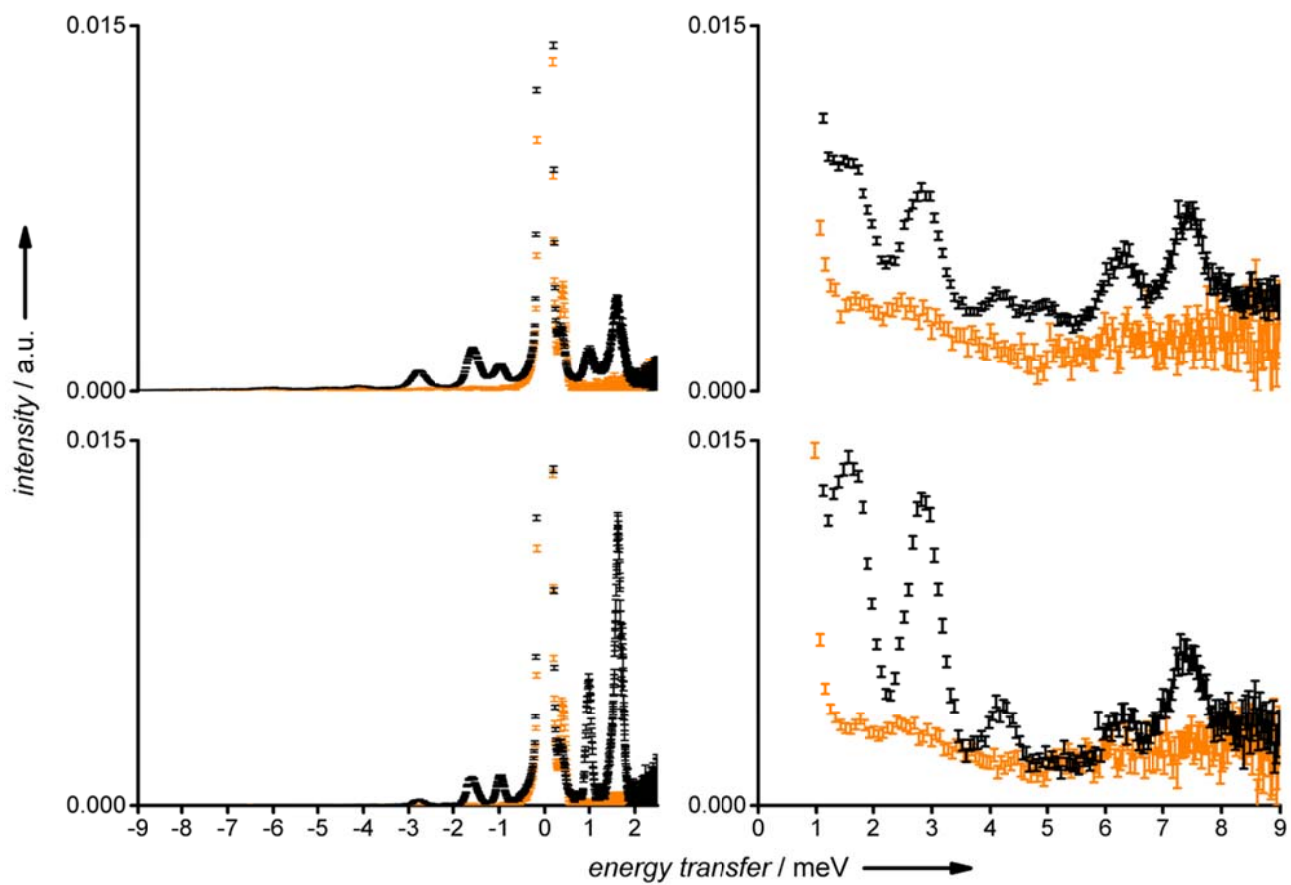


**Fig. S3** Bottom: INS spectra for  $\text{Y}^{\text{D}}$  (orange, 10 K) and  $\text{Tb}^{\text{D}}$  (black, 10 K). Top: INS spectra for  $\text{Y}^{\text{D}}$  (orange, 50 K) and  $\text{Tb}^{\text{D}}$  (black, 40 K). All spectra integrated over all  $Q$  range and normalised to the elastic line. Neutron wavelength  $\lambda = 4.74 \text{ \AA}$  (left) and  $\lambda = 2.37 \text{ \AA}$  (right).

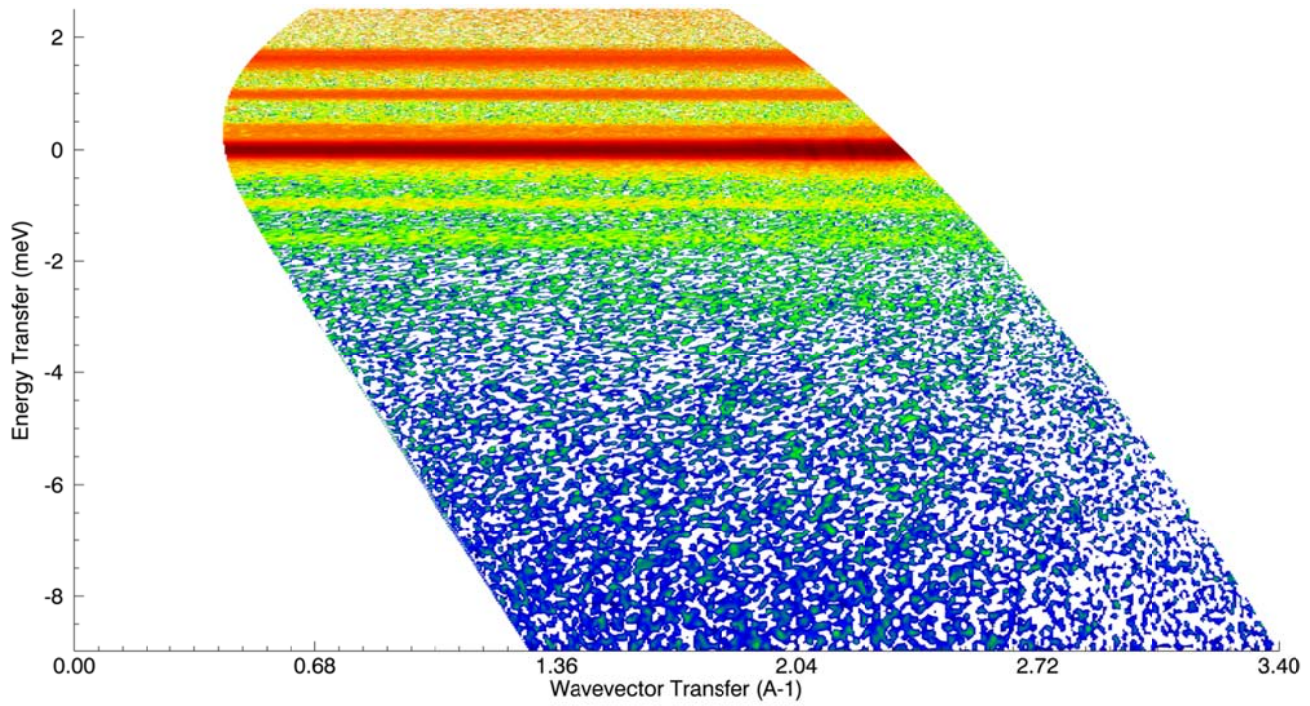


**Fig. S4**  $S(Q, \omega)$  diagram of **Tb** at 5 K and  $\lambda = 4.74$  Å neutron wavelength.

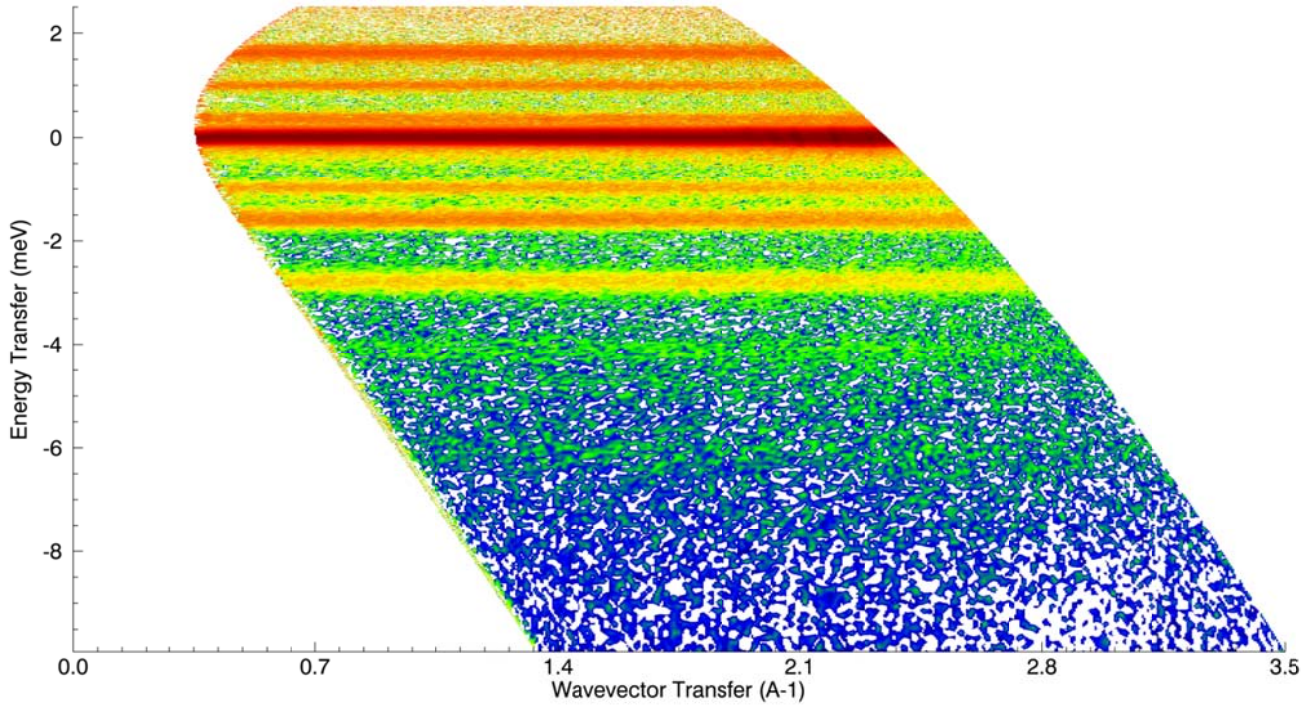


**Fig. S5**  $S(Q, \omega)$  diagram of **Tb** at 30 K and  $\lambda = 4.74$  Å neutron wavelength.

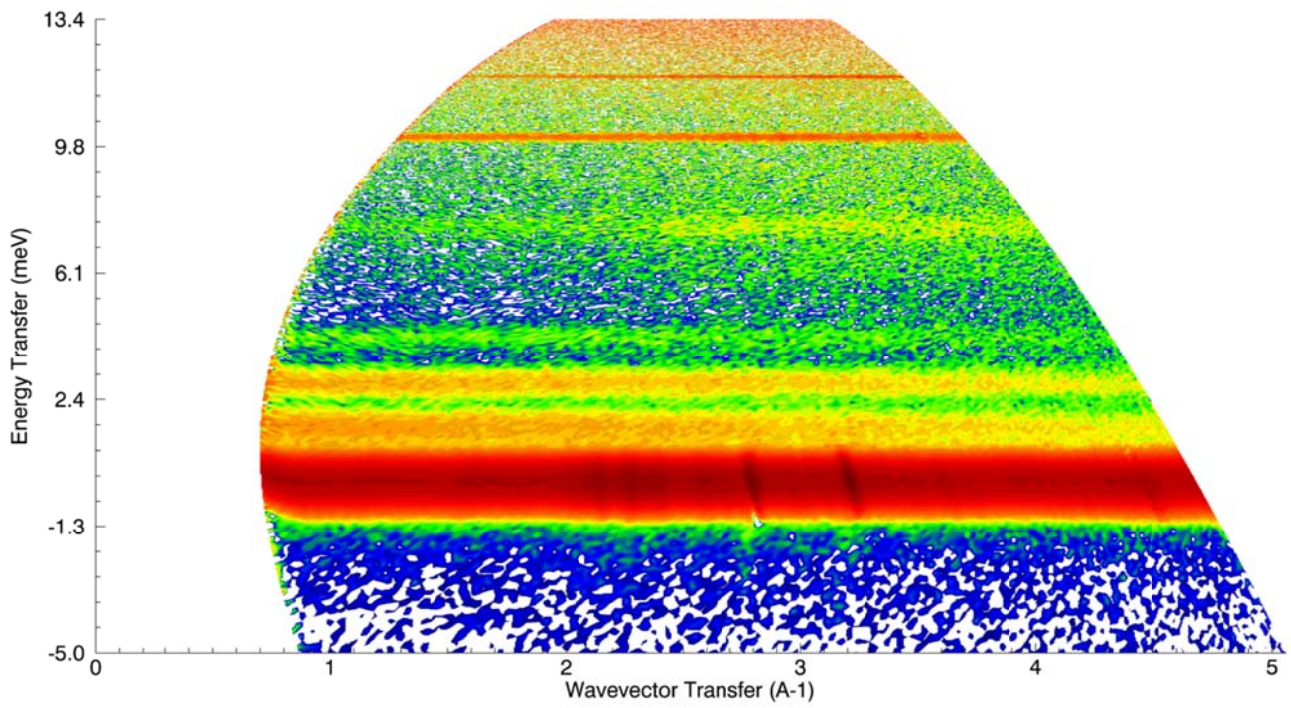


**Fig. S6**  $S(Q, \omega)$  diagram of **Tb** at 5 K and  $\lambda = 2.37 \text{ \AA}$  neutron wavelength.

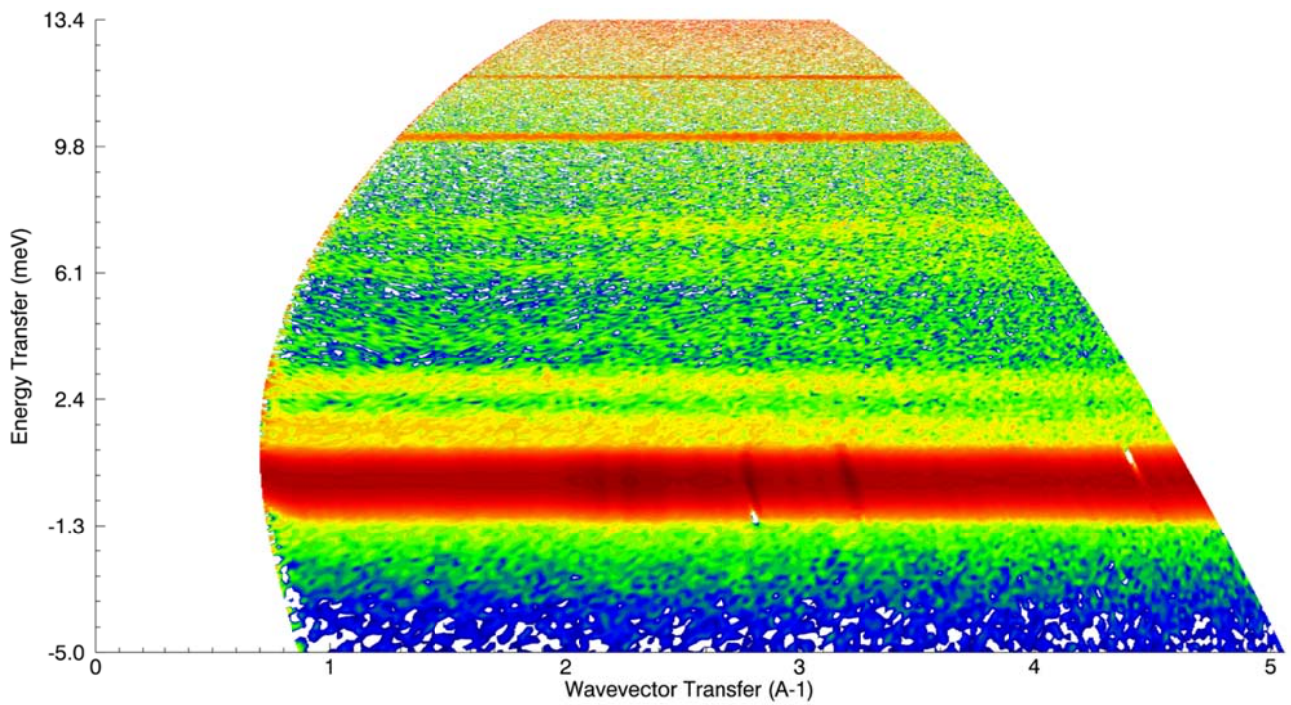


**Fig. S7**  $S(Q, \omega)$  diagram of **Tb** at 30 K and  $\lambda = 2.37 \text{ \AA}$  neutron wavelength.

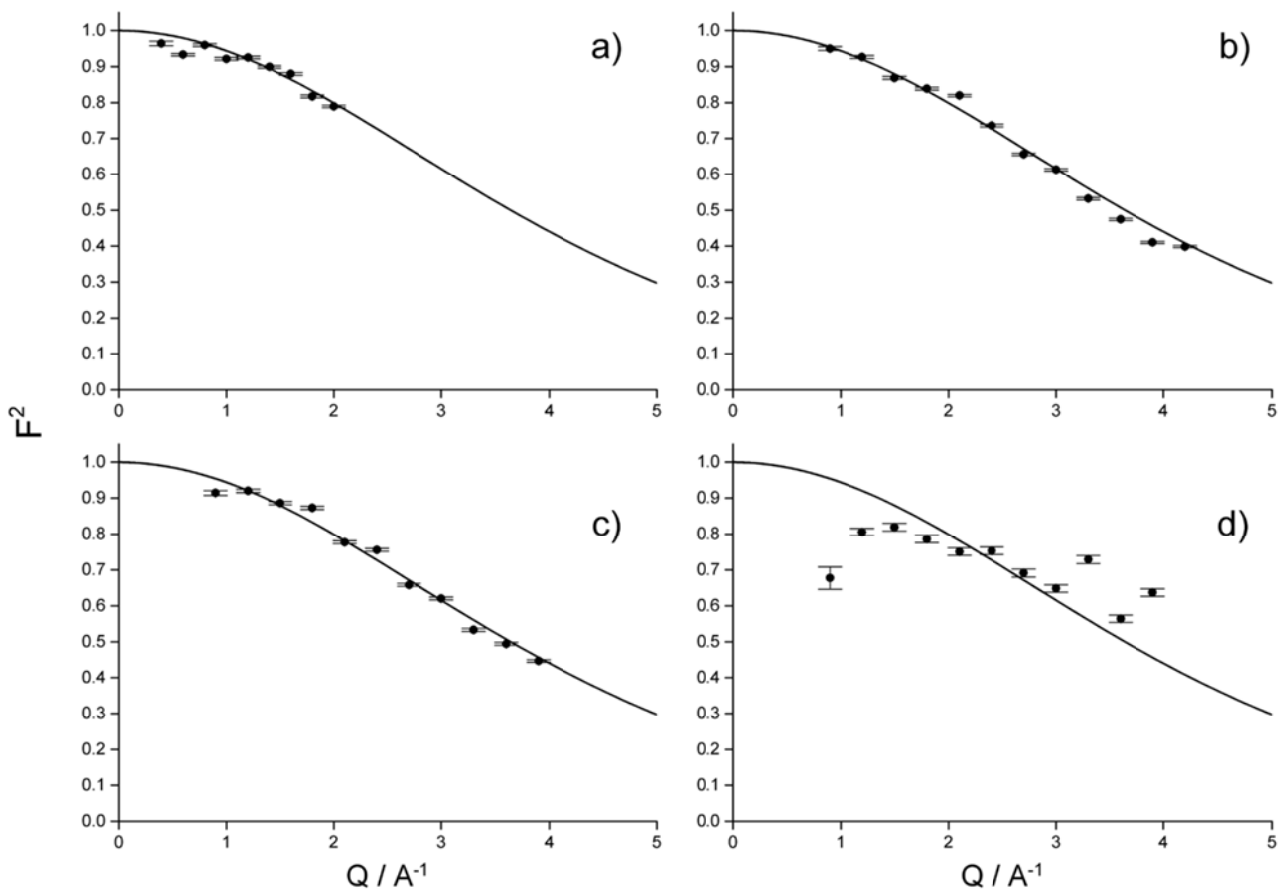


**Fig. S8** Q dependence of scattering intensity at energy corresponding to peaks Ia, IIa, Ib and IIb (5 K) for  $\text{Tb}^{\text{D}}$ . Theoretical  $F^2(Q)$  function for Tb(III) ion (solid line); a) peak Ib ( $\lambda = 4.74 \text{ \AA}$ , integration range  $0.9 \leq E \leq 1.1 \text{ meV}$ , binning interval =  $0.2 \text{ \AA}^{-1}$ ); b) peak Ia ( $\lambda = 2.37 \text{ \AA}$ , integration range  $1.2 \leq E \leq 2.0 \text{ meV}$ , binning interval =  $0.3 \text{ \AA}^{-1}$ ); c) peak IIa ( $\lambda = 2.37 \text{ \AA}$ , integration range  $2.4 \leq E \leq 3.2 \text{ meV}$ , binning interval =  $0.3 \text{ \AA}^{-1}$ ); d) peak IIb ( $\lambda = 2.37 \text{ \AA}$ , integration range  $4.1 \leq E \leq 4.3 \text{ meV}$ , binning interval =  $0.3 \text{ \AA}^{-1}$ )

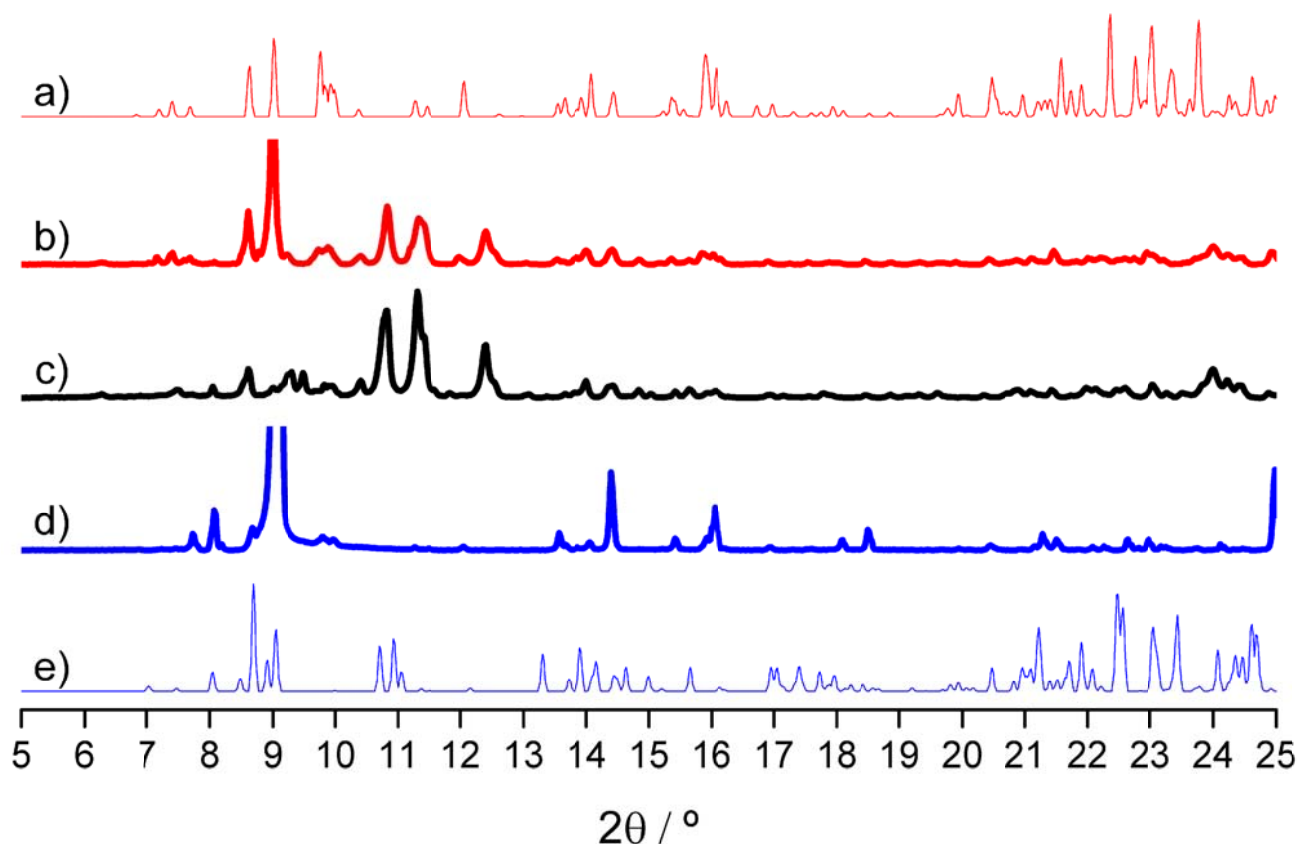


**Fig. S9** Powder X-ray diffraction patterns. a) Simulated for **Tb-a**. b) Experimental for **Tb-a**. c) Experimental for **Tb-b**. d) Experimental for **Tb-b**. e) Simulated for **Tb-b**

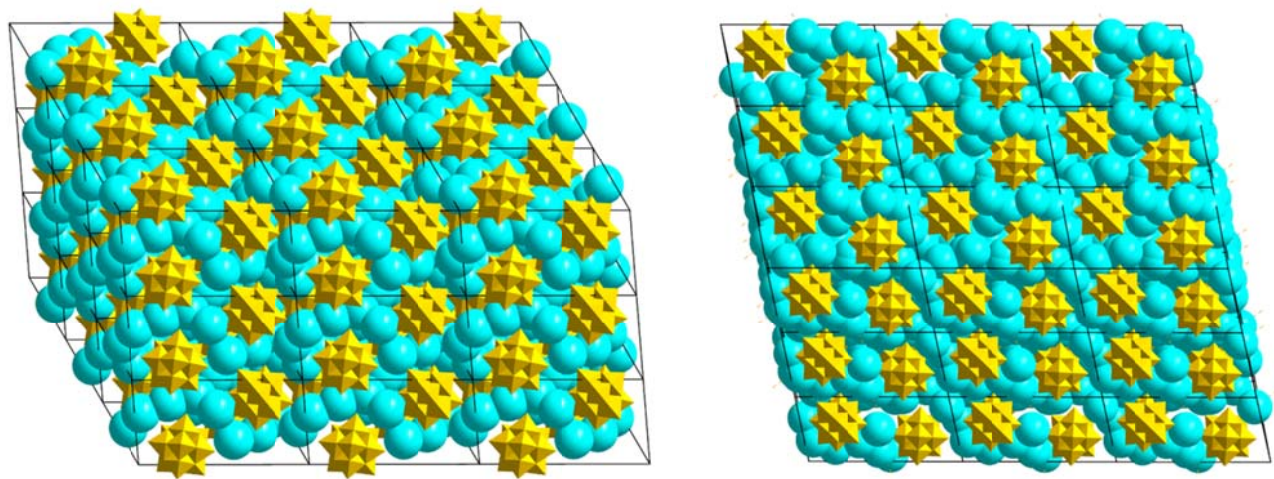


**Fig. S10** Crystal packing diagrams for **Tb-a** (left) and **Tb-b** (right) viewed along the pseudo C<sub>4</sub> molecular axis of [Tb(W<sub>5</sub>O<sub>18</sub>)<sub>2</sub>]<sup>9-</sup>. Water-coordinated sodium cations are represented as space-fill (turquoise) and WO<sub>6</sub> units as polyhedra (yellow). Oxygen atoms of Na-coordinating water molecules are omitted.

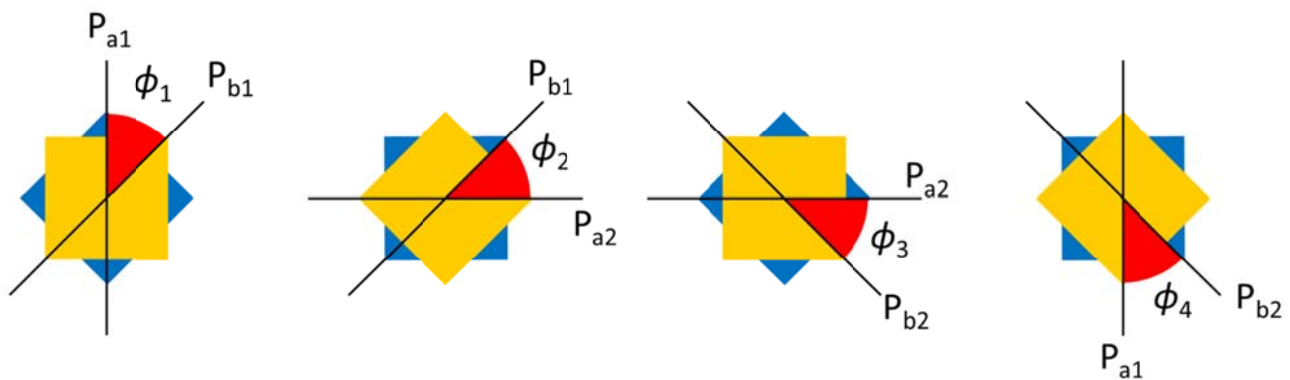


**Fig. S11** Representation of the four acute dihedral angles  $\phi_1$ ,  $\phi_2$ ,  $\phi_3$ , and  $\phi_4$  generated by the four pairs of planes O16-Ln-O18/O19-Ln-O21 (P<sub>a1</sub>/P<sub>b1</sub>), O16-Ln-O18/O20-Ln-O22 (P<sub>a1</sub>/P<sub>b2</sub>), O15-Ln-O17/O19-Ln-O21 (P<sub>a2</sub>/P<sub>b1</sub>), O15-Ln-O17/O20-Ln-O22 (P<sub>a2</sub>/P<sub>b2</sub>). The average deviation from the ideal value of 45° of the skew angle between the two bases of the antiprism is here defined as the average deviation from 45° ( $AD(\phi)_{45}$ ) calculated over  $\phi_1$ ,  $\phi_2$ ,  $\phi_3$ , and  $\phi_4$ :

$$AD(\phi)_{45} = \frac{\sum_{i=1}^4 |\phi_i - 45|}{4}$$

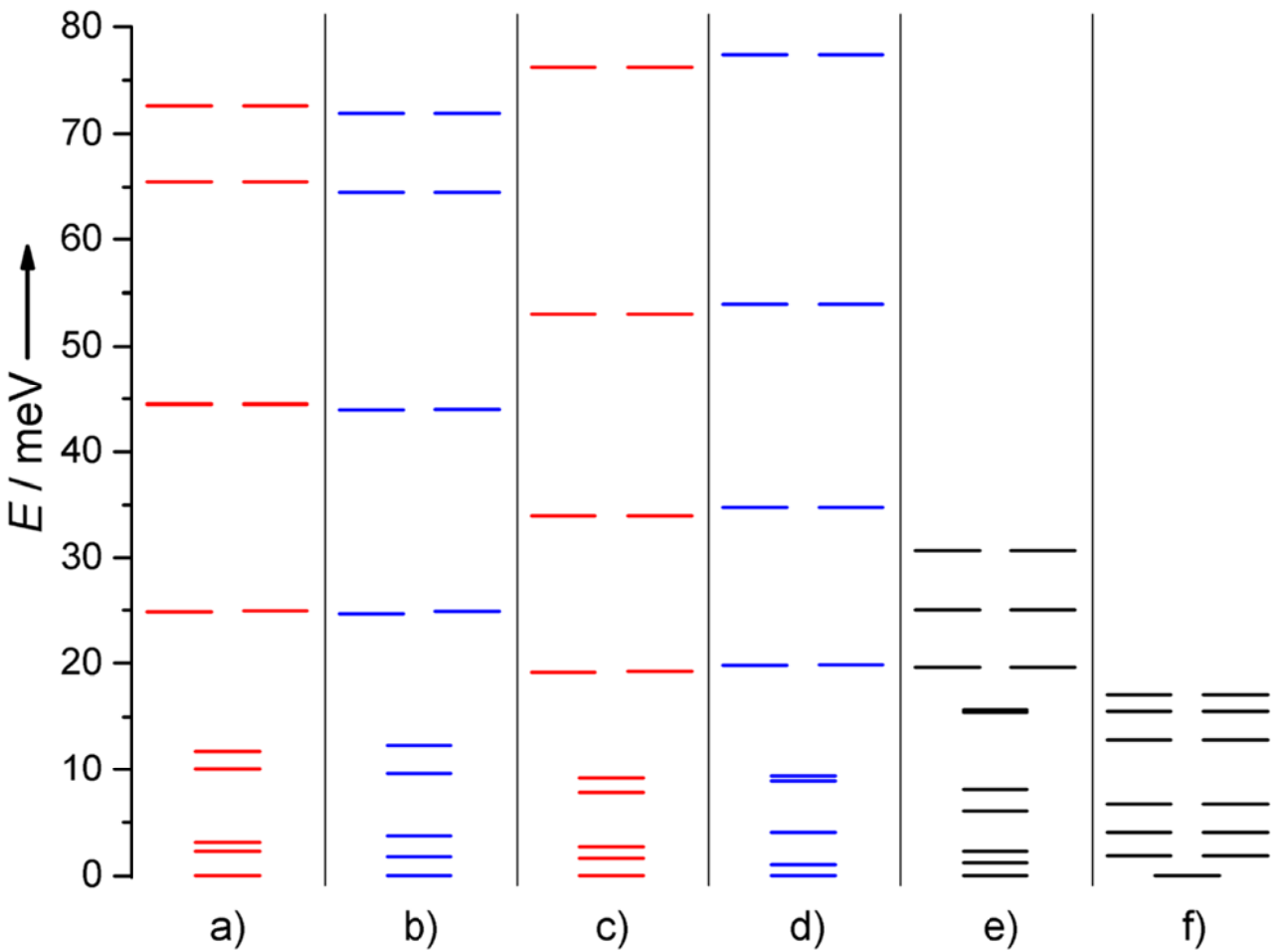


**Fig. S12** a) Detail of the energies of the low lying states corresponding to the  $J = 6$  ground state multiplet obtained from CASSCF/RASSI *ab initio* calculation for **Tb-a**. b) Detail of the energies of the low lying states corresponding to the  $J = 6$  ground state multiplet obtained from CASSCF/RASSI *ab initio* calculation for **Tb-b**. c)  $J = 6$  ground state multiplet energies obtained from the simplified CF Hamiltonian with fitted crystal field parameters for **Tb-a**. d)  $J = 6$  ground state multiplet energies obtained from the simplified CF Hamiltonian with fitted crystal field parameters for **Tb-b**. e)  $J = 6$  ground state multiplet energies literature values for **Tb-a**, the crystal field parameters that give rise to these energy levels were not explicitly reported.<sup>16</sup> f)  $J = 6$  ground state multiplet energies literature values for **Tb-a**; crystal field parameters ( $\text{cm}^{-1}$ )  $A_2^0 r^2 = -36.8$ ,  $A_4^0 r^4 = -89.0$ ,  $A_6^0 r^6 = -5.2$  with Hamiltonian  $\hat{H}_{\text{CF}} = A_2^0 r^2 \alpha \hat{O}_2^0 + A_4^0 r^4 \beta \hat{O}_4^0 + A_6^0 r^6 \gamma \hat{O}_6^0$ .<sup>17</sup>

**Table S2.** CASSCF/RASSI spin-orbit energies for the low-lying multiplets of **Tb-a** and **Tb-b**.

		<b>Tb-a</b>		<b>Tb-b</b>	
		cm <sup>-1</sup>	meV	cm <sup>-1</sup>	meV
<sup>7</sup> F <sub>6</sub>	1	0	0	0	0
	2	18.466	2.28936	14.352	1.77932
	3	25.147	3.11765	30.229	3.74771
	4	81.752	10.13538	78.352	9.71386
	5	94.735	11.74498	99.566	12.34391
	6	200.811	24.89598	199.459	24.72837
	7	201.413	24.97062	201.099	24.93169
	8	358.782	44.48078	354.728	43.97818
	9	358.941	44.5005	355.13	44.02802
	10	527.501	65.39809	519.765	64.439
	11	527.505	65.39859	519.772	64.43987
	12	586.067	72.65894	580.385	71.9545
	13	586.067	72.65894	580.385	71.9545
<sup>7</sup> F <sub>5</sub>	14	2209.368	273.91123	2209.583	273.93789
	15	2230.01	276.47037	2226.291	276.0093
	16	2231.993	276.71622	2231.31	276.63154
	17	2269.215	281.3309	2259.784	280.16167
	18	2269.967	281.42413	2267.341	281.09856
	19	2271.702	281.63923	2270.141	281.4457
	20	2294.313	284.44247	2298.68	284.98388
	21	2306.181	285.91384	2304.035	285.64778
	22	2307.285	286.05071	2308.036	286.14381
	23	2576.219	319.39239	2569.276	318.53161
	24	2576.24	319.39499	2569.33	318.53831
<sup>7</sup> F <sub>4</sub>	25	3596.143	445.8397	3593.763	445.54463
	26	3602.897	446.67704	3604.69	446.89933
	27	3643.502	451.71113	3642.266	451.5579
	28	3644.484	451.83288	3642.869	451.63266
	29	3738.093	463.43826	3733.899	462.9183
	30	3741.218	463.82569	3739.921	463.66489
	31	3810.095	472.36486	3792.573	470.19254
	32	3836.758	475.67047	3831.79	475.05455
	33	3850.225	477.34007	3858.478	478.36325

**Table S3.** Complex amplitudes of the CASSCF/RASSI wavefunctions corresponding to the lowest atomic multiplet  $J = 6$  on the basis of total angular momentum eigenstates  $|JM\rangle$  for **Tb-a**. The reference system has the origin on the Tb(III) ion and is oriented along the main axes of the  $g$ -tensor calculated for the first excited pseudo-doublet of **Tb-a**.

<b> JM &gt;</b>	<b>w.f. 1</b>	<b>w.f. 2</b>	<b>w.f. 3</b>	<b>w.f. 4</b>
-6	-0.000031 -0.000002	-0.000167 0.000299	0.000447 0.000005	-0.000952 -0.001289
-5	-0.001099 0.000002	0.000293 0.004183	0.001910 -0.003914	-0.005202 0.003329
-4	-0.010118 0.009067	0.007381 -0.003644	-0.006176 -0.000140	-0.004284 -0.003992
-3	0.010763 0.003626	0.020538 -0.014014	0.015953 -0.023712	-0.002691 0.024183
-2	0.011448 0.035297	-0.006767 -0.021069	-0.021356 0.016082	0.439397 0.552293
-1	0.021599 -0.022673	-0.449709 -0.544248	0.109177 0.697029	-0.021499 -0.010748
0	0.032393 -0.996798	0.013610 0.023230	-0.035833 -0.000220	-0.016334 0.032367
1	0.020081 0.024027	0.254912 0.658380	-0.117719 0.695637	-0.021418 -0.010909
2	-0.013716 0.034479	-0.015071 -0.016204	-0.021157 -0.016343	-0.705305 -0.025365
3	0.010975 -0.002920	0.022267 -0.011065	-0.015661 -0.023906	0.017855 -0.016531
4	0.009508 0.009705	-0.006787 0.004657	-0.006177 0.000064	0.005756 0.001075
5	-0.001096 -0.000073	-0.003505 -0.002301	-0.001862 -0.003937	-0.000412 -0.006163
6	0.000031 0.000000	0.000342 0.000000	0.000447 0.000000	0.001603 0.000000
<b> JM &gt;</b>	<b>w.f. 5</b>	<b>w.f. 6</b>	<b>w.f. 7</b>	<b>w.f. 8</b>
-6	0.000989 0.001324	-0.004571 -0.001969	-0.004547 -0.001930	-0.001672 -0.001202
-5	0.005323 -0.003317	0.000642 -0.003705	0.001114 -0.003791	-0.007125 0.039120
-4	0.005906 0.004841	-0.026064 0.010179	-0.026373 0.009748	0.317073 0.630078
-3	0.002493 -0.024554	-0.316411 0.631119	-0.314271 0.631179	-0.026320 -0.009656
-2	-0.439708 -0.551904	-0.007357 -0.023216	-0.009042 -0.023156	0.001344 0.006035
-1	0.024922 -0.006850	0.010199 -0.007336	-0.024508 0.025542	-0.006094 0.004362
0	-0.032999 -0.016534	-0.000051 0.000245	-0.016657 -0.003389	0.000284 -0.000881
1	-0.009433 -0.024064	0.006465 0.010772	0.012579 0.033088	-0.002402 -0.007099
2	-0.705313 -0.021792	0.015941 -0.018413	-0.017371 0.017782	-0.004614 0.004116
3	0.018175 -0.016697	-0.040945 -0.704805	0.042655 0.703800	-0.027008 -0.007521
4	0.007413 0.001832	0.019912 0.019659	-0.020467 -0.019279	-0.625212 0.326564
5	-0.000530 -0.006250	-0.000876 0.003656	0.000456 -0.003925	0.017047 -0.035924
6	0.001652 0.000000	0.004977 0.000000	-0.004939 0.000000	0.002059 0.000000
<b> JM &gt;</b>	<b>w.f. 9</b>	<b>w.f. 10</b>	<b>w.f. 11</b>	<b>w.f. 12</b>
-6	0.001687 0.001201	0.037352 -0.132782	0.037365 -0.132785	-0.693147 -0.022122
-5	0.007028 -0.039144	-0.114731 -0.682804	-0.114700 -0.682803	0.126325 -0.054838
-4	-0.318411 -0.629252	0.028687 0.026447	0.028696 0.026436	-0.005402 0.005633
-3	0.026488 0.009278	-0.000168 -0.003212	-0.000091 -0.003391	0.001128 -0.005263
-2	-0.002287 -0.006006	0.006128 -0.001708	0.006350 -0.001754	-0.000937 0.001278
-1	0.005787 -0.004908	-0.003227 -0.002443	-0.003417 -0.002616	0.000326 -0.000450
0	-0.018293 -0.005847	0.000181 0.000239	0.000176 -0.000134	-0.000001 0.000065
1	-0.001867 -0.007355	0.001478 0.003768	-0.001592 -0.003998	0.000312 0.000460
2	-0.005346 0.003566	-0.003303 0.005437	0.003409 -0.005638	0.000896 0.001307
3	-0.026958 -0.007805	0.003046 0.001032	-0.003240 -0.001006	0.000959 0.005297
4	-0.624349 0.327919	0.017690 0.034776	-0.017674 -0.034784	0.005219 0.005803
5	0.016978 -0.035964	0.626225 0.295341	-0.626206 -0.295368	0.124511 0.058840
6	0.002071 0.000000	-0.137936 0.000000	0.137942 0.000000	0.693500 0.000000
<b> JM &gt;</b>	<b>w.f. 13</b>	--	--	--
-6	0.693145 0.022124			
-5	-0.126328 0.054845			
-4	0.005405 -0.005627			
-3	-0.001133 0.005291			
-2	0.000933 -0.001230			
-1	-0.000395 0.000582			
0	0.000069 0.000001			
1	0.000376 0.000594			
2	0.000893 0.001259			
3	0.000963 0.005324			
4	0.005223 0.005796			
5	0.124515 0.058847			
6	0.693498 0.000000			

**Table S4.** Complex amplitudes of the CASSCF/RASSI wavefunctions corresponding to the lowest atomic multiplet  $J = 6$  on the basis of total angular momentum eigenstates  $|JM\rangle$  for **Tb-b**. The reference system has the origin on the Tb(III) ion and is oriented along the main axes of the  $g$ -tensor calculated for the first excited pseudo-doublet of **Tb-b**.

<b> JM &gt;</b>	<b>w.f. 1</b>	<b>w.f. 2</b>	<b>w.f. 3</b>	<b>w.f. 4</b>
-6	-0.000151 -0.000176	-0.000195 -0.000132	0.000059 0.000308	-0.000698 0.000791
-5	0.000326 0.000325	-0.004116 -0.004434	0.001857 0.005176	0.001235 0.002200
-4	0.012373 0.016214	-0.001104 0.002528	0.003757 -0.002602	-0.012718 -0.007041
-3	0.004232 -0.005344	0.035347 0.000518	-0.006108 0.059030	0.003793 -0.024392
-2	-0.047816 0.072362	0.023378 -0.009784	-0.020721 -0.007818	0.547354 0.443186
-1	-0.031135 0.006993	-0.247825 0.660523	0.482615 -0.512149	0.019029 -0.013250
0	0.413276 -0.900664	-0.007818 0.025476	-0.029322 -0.024196	0.066027 -0.029799
1	-0.015004 -0.028164	0.165359 -0.685832	0.411216 -0.571065	-0.022525 0.005504
2	-0.023675 0.083439	-0.013865 -0.021214	-0.011610 -0.018860	0.029770 -0.703651
3	-0.001291 0.006693	0.029553 0.019399	-0.056797 0.017203	-0.020801 -0.013292
4	-0.020361 0.001193	-0.000504 0.002712	-0.001841 0.004182	-0.003134 0.014195
5	0.000460 0.000035	-0.005894 0.001361	-0.005434 -0.000841	0.000833 0.002382
6	0.000232 0.000000	0.000236 0.000000	0.000313 0.000000	-0.001054 0.000000
<b> JM &gt;</b>	<b>w.f. 5</b>	<b>w.f. 6</b>	<b>w.f. 7</b>	<b>w.f. 8</b>
-6	0.000655 -0.000878	-0.000671 -0.001989	-0.000623 -0.002058	-0.007521 -0.003971
-5	-0.001224 -0.002310	0.009462 -0.000617	0.010166 -0.001342	0.020507 -0.037507
-4	0.016893 0.009213	0.010857 0.027249	0.010082 0.027274	0.479502 0.516760
-3	-0.001778 0.025425	-0.701219 -0.081049	-0.696610 -0.091814	0.028838 -0.008353
-2	-0.566801 -0.414965	-0.016424 0.019462	-0.014554 0.022518	0.010502 0.010891
-1	-0.025492 0.007849	0.009379 0.001724	-0.067106 -0.010998	-0.001372 -0.002111
0	-0.043947 -0.087590	0.006092 0.004373	-0.002100 0.002829	-0.000609 -0.000151
1	-0.021530 0.015744	-0.004633 -0.008335	-0.029963 -0.061044	0.002199 -0.001227
2	0.006153 -0.702439	0.013187 -0.021785	-0.017338 0.020452	0.014372 -0.004728
3	-0.021445 -0.013773	0.301056 0.638469	-0.289638 -0.640160	-0.021602 -0.020850
4	-0.002712 0.019050	0.029290 0.001572	-0.029025 -0.001750	0.665297 -0.233116
5	0.001120 0.002362	-0.002442 -0.009163	0.001659 0.010119	-0.000624 -0.042742
6	-0.001095 0.000000	-0.002099 0.000000	0.002150 0.000000	-0.008505 0.000000
<b> JM &gt;</b>	<b>w.f. 9</b>	<b>w.f. 10</b>	<b>w.f. 11</b>	<b>w.f. 12</b>
-6	-0.007547 -0.003960	-0.132911 -0.077459	-0.132921 -0.077455	0.302195 -0.620431
-5	0.020451 -0.037599	0.364139 -0.584558	0.364115 -0.584553	-0.136473 -0.071509
-4	0.479932 0.515859	-0.028105 -0.033694	-0.028186 -0.033727	-0.000831 0.000609
-3	0.028899 -0.008288	0.004971 -0.006625	0.005369 -0.006845	-0.000371 0.000286
-2	0.010024 0.013026	-0.001066 0.000964	-0.001030 0.000952	0.001432 0.000504
-1	0.000813 -0.003409	0.005795 0.000239	0.006231 0.000497	0.000303 -0.001290
0	-0.007289 0.029577	0.000879 0.000237	0.000464 -0.001718	-0.000009 0.000006
1	-0.000864 0.003396	-0.005127 -0.002711	0.005634 0.002708	-0.001292 -0.000293
2	-0.014929 0.006877	-0.000435 -0.001370	0.000410 0.001341	0.000174 -0.001509
3	0.021739 0.020767	-0.000959 -0.008226	0.001193 0.008618	0.000420 -0.000208
4	-0.664668 0.233799	-0.041248 0.014960	0.041334 -0.014949	-0.000911 0.000481
5	0.000639 0.042796	-0.020274 -0.688399	0.020292 0.688383	-0.004528 -0.154007
6	0.008523 0.000000	-0.153835 0.000000	0.153841 0.000000	0.690113 0.000000
<b> JM &gt;</b>	<b>w.f. 13</b>	--	--	--
-6	-0.302191 0.620432			
-5	0.136473 0.071517			
-4	0.000835 -0.000607			
-3	0.000311 -0.000220			
-2	-0.001485 -0.000538			
-1	-0.000324 0.001284			
0	0.000118 0.000188			
1	-0.001297 -0.000271			
2	0.000167 -0.001571			
3	0.000334 -0.000183			
4	-0.000911 0.000485			
5	-0.004536 -0.154010			
6	0.690112 0.000000			

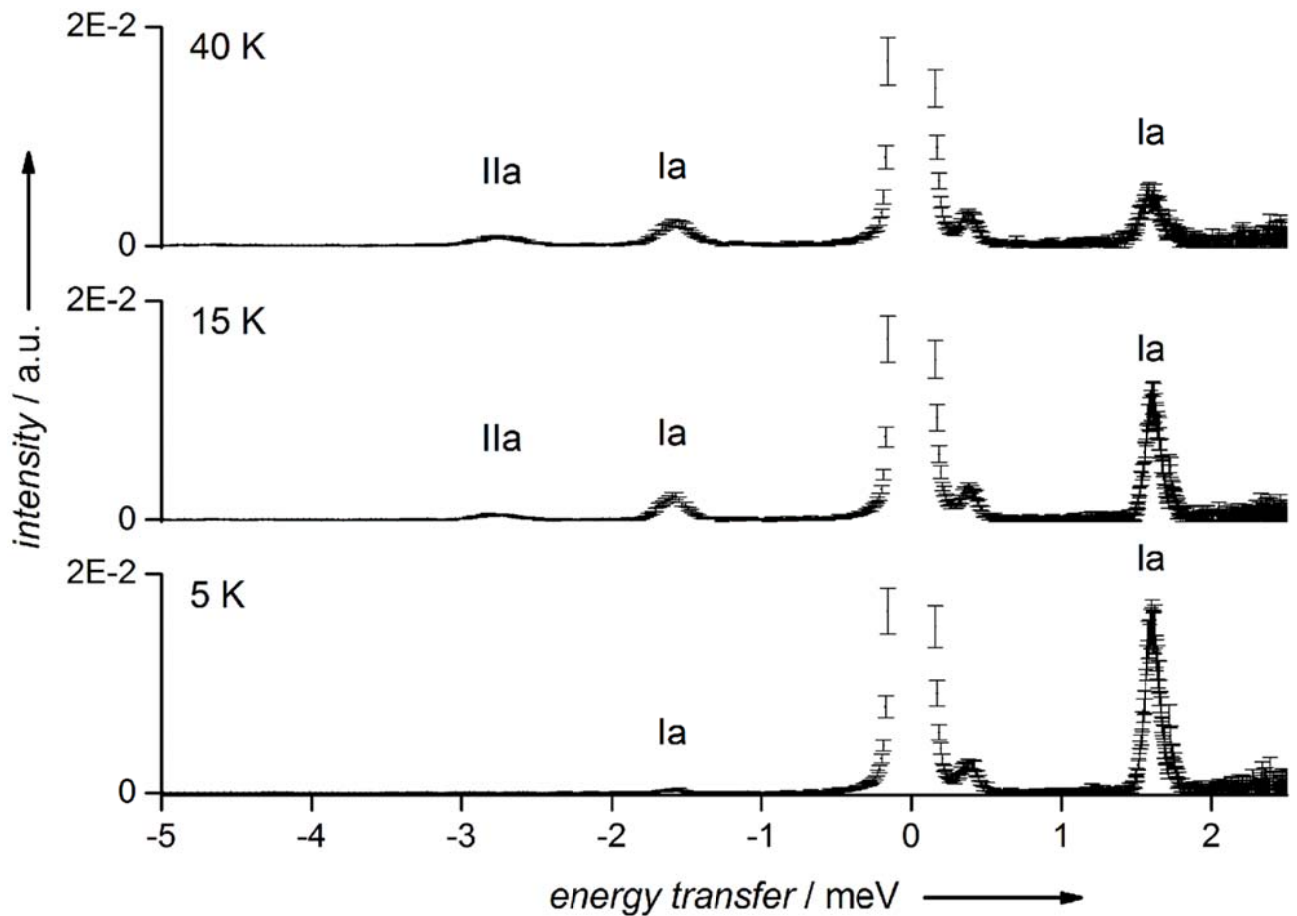


**Fig. S13** Variable temperature INS spectra for **Tb-aP**. Data collected at  $\lambda = 4.74 \text{ \AA}$ , integration range  $0.8 \text{ \AA}^{-1} < Q < 2.4 \text{ \AA}^{-1}$ .

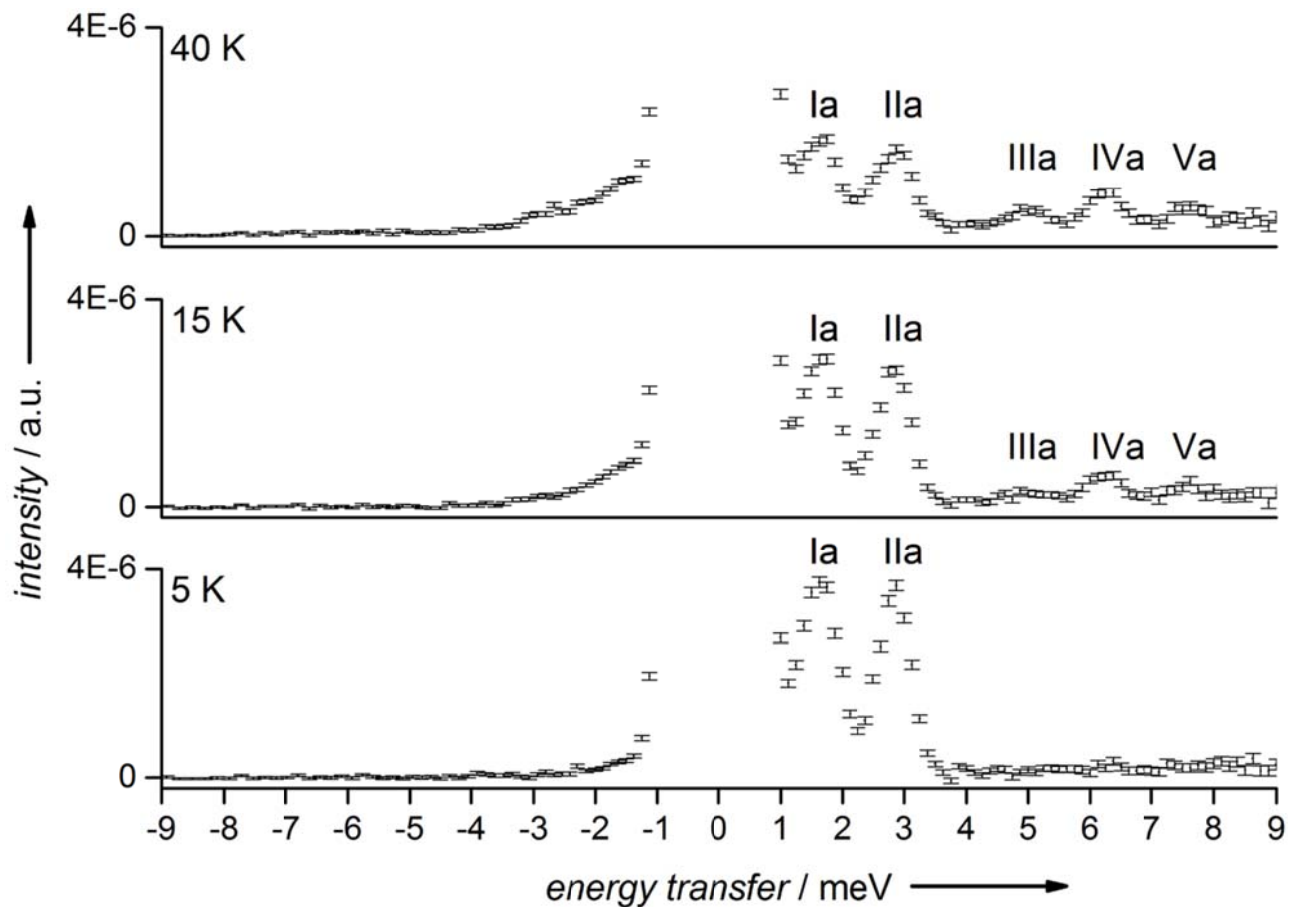


**Fig. S14** Variable temperature INS spectra for **Tb-a<sup>P</sup>**. Data collected at  $\lambda = 2.37 \text{ \AA}$ , integration range  $0.8 \text{ \AA}^{-1} < Q < 2.4 \text{ \AA}^{-1}$ , binning interval 0.125 meV.

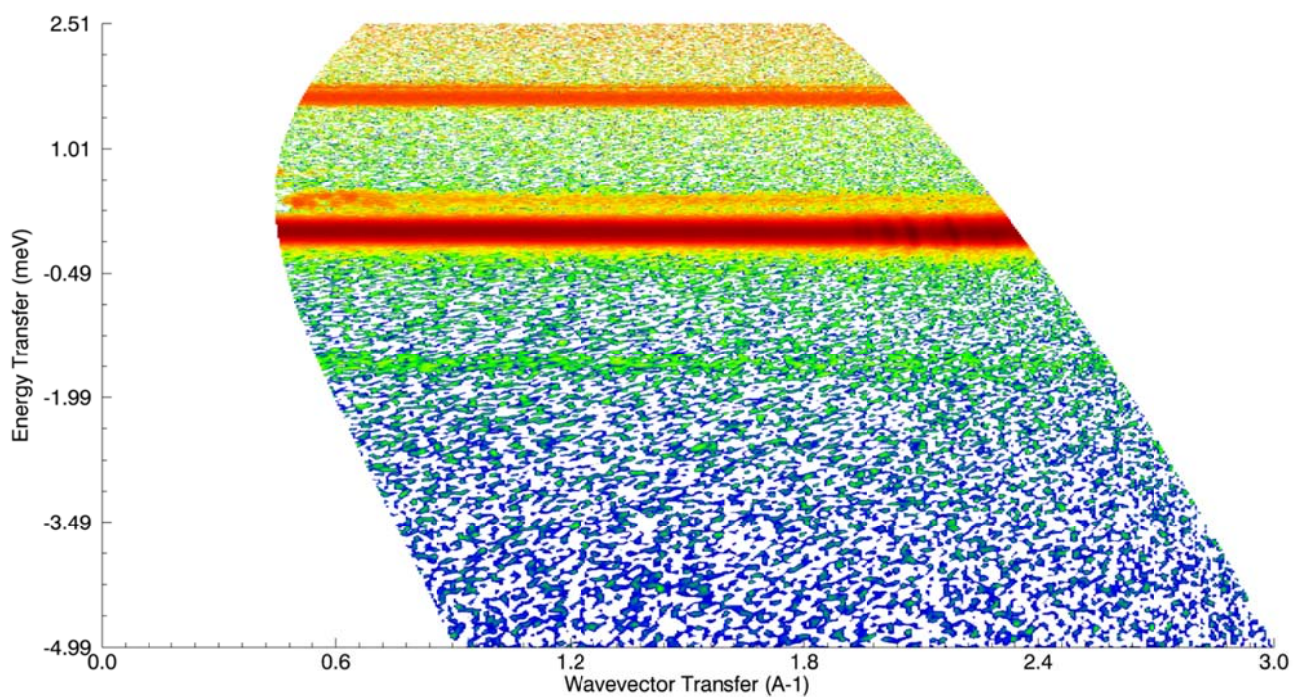


**Fig. S15**  $S(Q, \omega)$  diagram of  $\text{Tb-a}^{\text{D}}$  at 5 K and  $\lambda = 4.74 \text{ \AA}$  neutron wavelength.

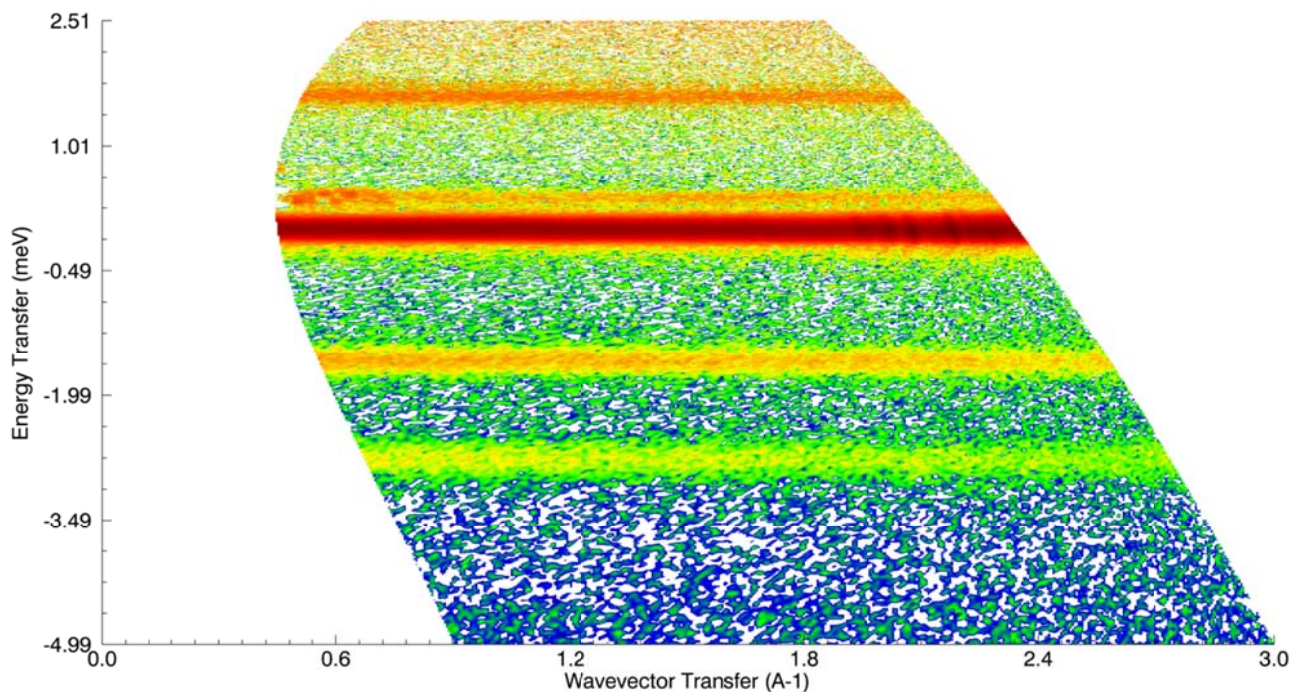


**Fig. S16**  $S(Q, \omega)$  diagram of  $\text{Tb-a}^{\text{D}}$  at 40 K and  $\lambda = 4.74 \text{ \AA}$  neutron wavelength.

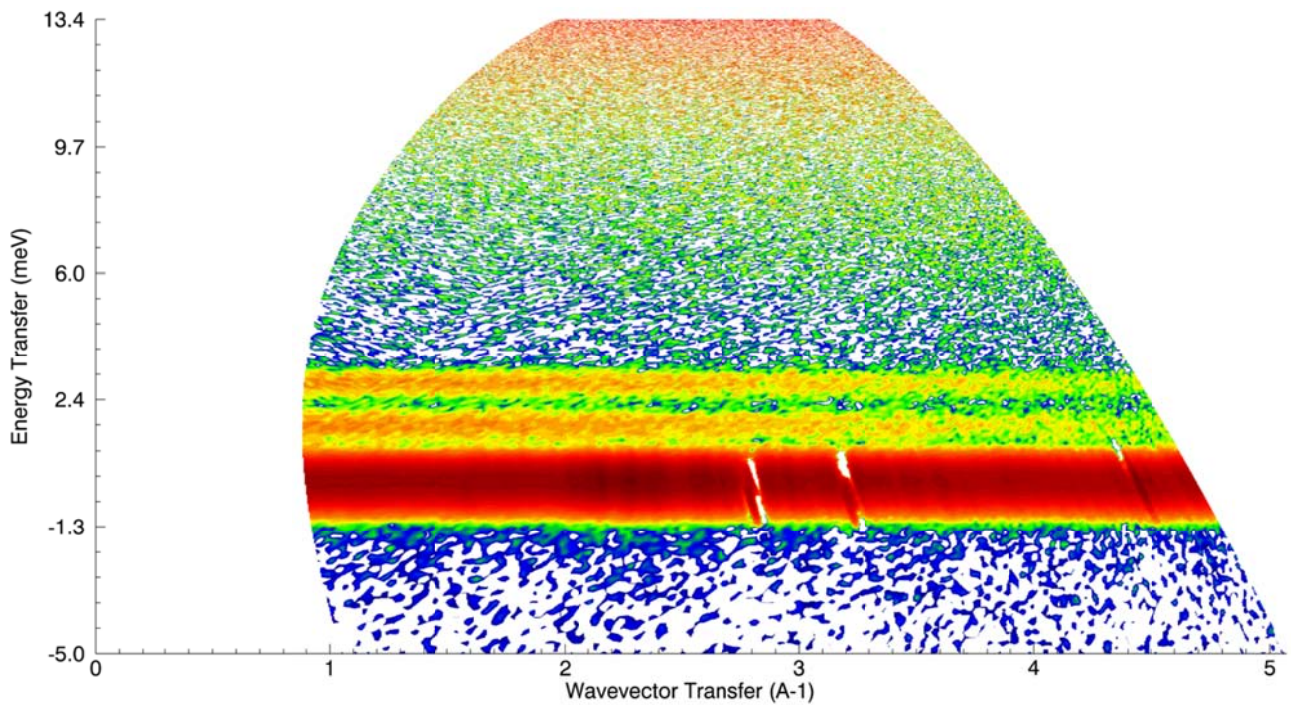


**Fig. S17**  $S(Q, \omega)$  diagram of  $\text{Tb-a}^{\text{D}}$  at 5 K and  $\lambda = 2.37 \text{ \AA}$  neutron wavelength.

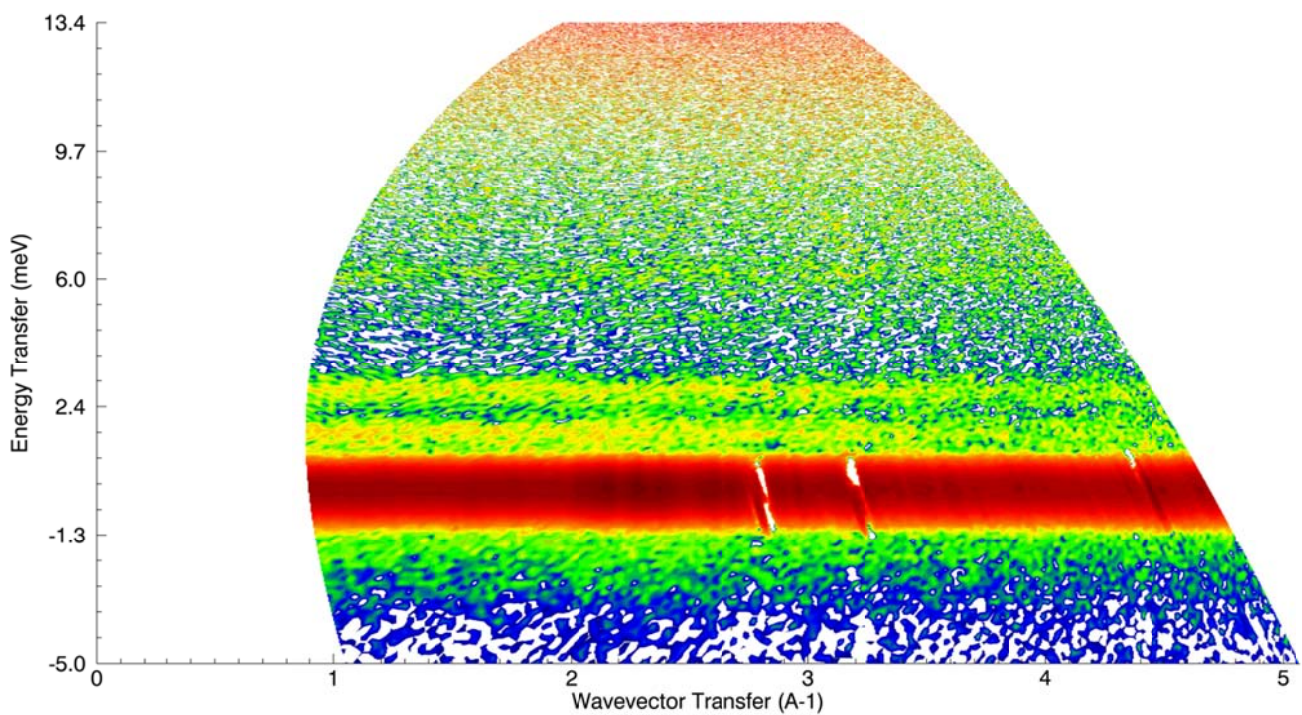


**Fig. S18**  $S(Q, \omega)$  diagram of  $\text{Tb-a}^{\text{D}}$  at 40 K and  $\lambda = 2.37 \text{ \AA}$  neutron wavelength.

**Table S5.** CASSCF/RASSI B(k,q) crystal field parameters (meV) for the Extended Stevens Operators (ESO) as computed by the SINGLE\_ANISO module of Molcas, with k the rank and q the component of the operator. The reference system has the origin on the Tb(III) ion and is oriented along the main axes of the g-tensor calculated for the first excited pseudo-doublet of **Tb-a** and **Tb-b** respectively.

**Tb-a**

k	q	B(k,q)
2	-2	0.00364
2	-1	0.05851
2	0	0.71028
2	1	-0.08244
2	2	0.01852

4	-4	-6.53997E-4
4	-3	0.00169
4	-2	-3.79475E-5
4	-1	1.09886E-4
4	0	-0.00122
4	1	-5.0348E-4
4	2	-3.31725E-5
4	3	1.95295E-4
4	4	5.98773E-4

6	-6	-6.21112E-8
6	-5	-2.93668E-6
6	-4	3.21245E-6
6	-3	9.94548E-7
6	-2	-2.52274E-7
6	-1	-1.97598E-6
6	0	-7.51428E-6
6	1	-1.7076E-6
6	2	-3.75784E-7
6	3	-2.49986E-6
6	4	-3.59595E-7
6	5	-6.18049E-7
6	6	3.07338E-7

**Tb-b**

k	q	B(k,q)
2	-2	1.42972E-4
2	-1	-0.10409
2	0	0.70018
2	1	0.02901
2	2	0.04564

4	-4	0.00117
4	-3	2.58863E-5
4	-2	6.68707E-5
4	-1	-6.64415E-4
4	0	-0.00119
4	1	-1.58559E-4
4	2	-1.0613E-4
4	3	-5.48863E-4
4	4	7.10936E-4

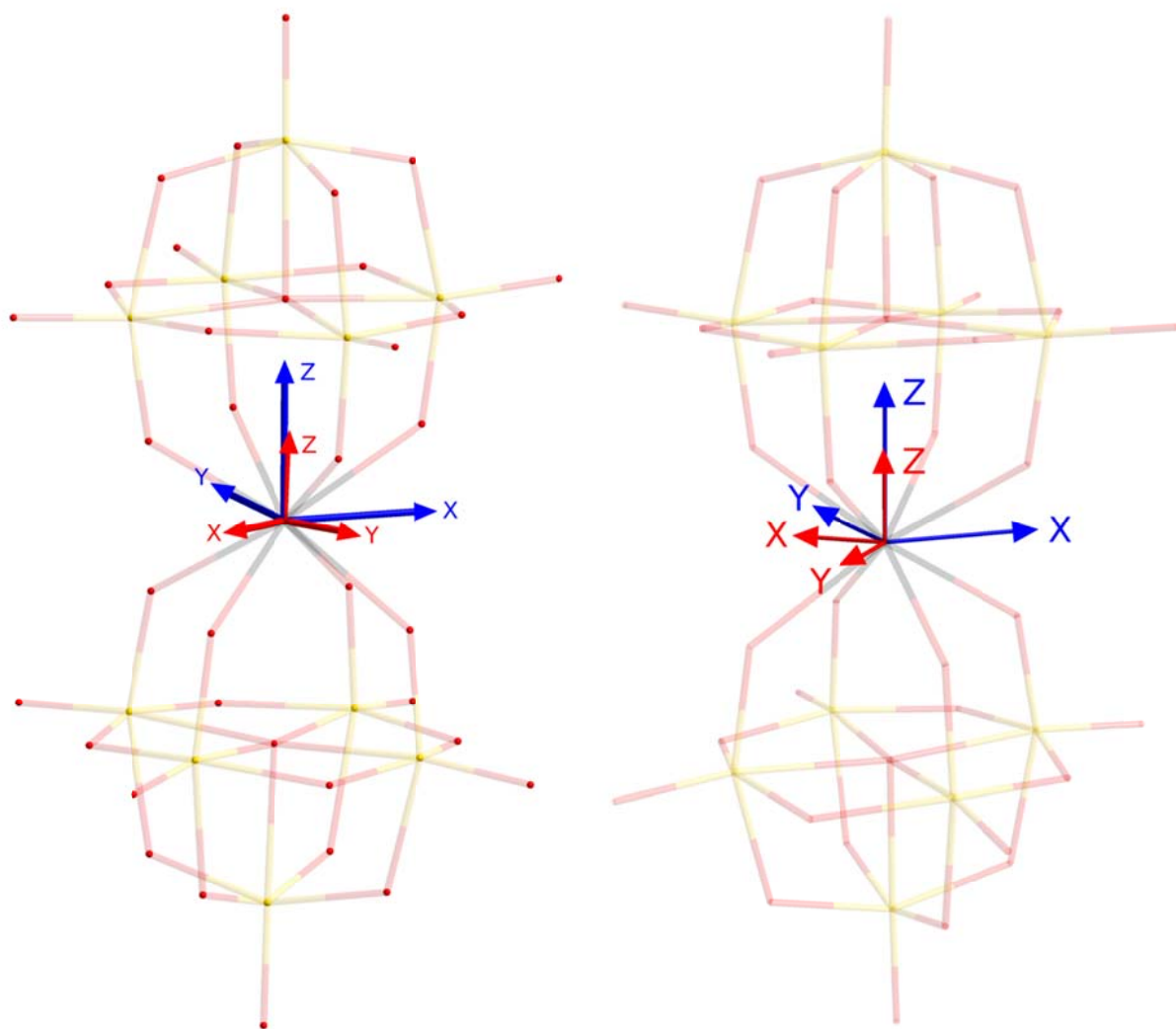
6	-6	2.28334E-8
6	-5	3.74757E-6
6	-4	-4.35004E-6
6	-3	3.64135E-6
6	-2	6.89233E-8
6	-1	-2.44123E-6
6	0	-7.22833E-6
6	1	-3.5608E-6
6	2	-6.59497E-7
6	3	2.32893E-6
6	4	-3.86924E-6
6	5	4.3616E-6
6	6	-1.04473E-9

**Table S6.** Cartesian coordinates ( $\text{\AA}$ ) used as inputs in the CASSCF/RASSI/SINGLE\_ANISO calculations for **Tb-a** and **Tb-b** (a) and orientation of the first excited pseudo doublet g-tensor axes in the molecular reference system for **Tb-a** and **Tb-b** (b).

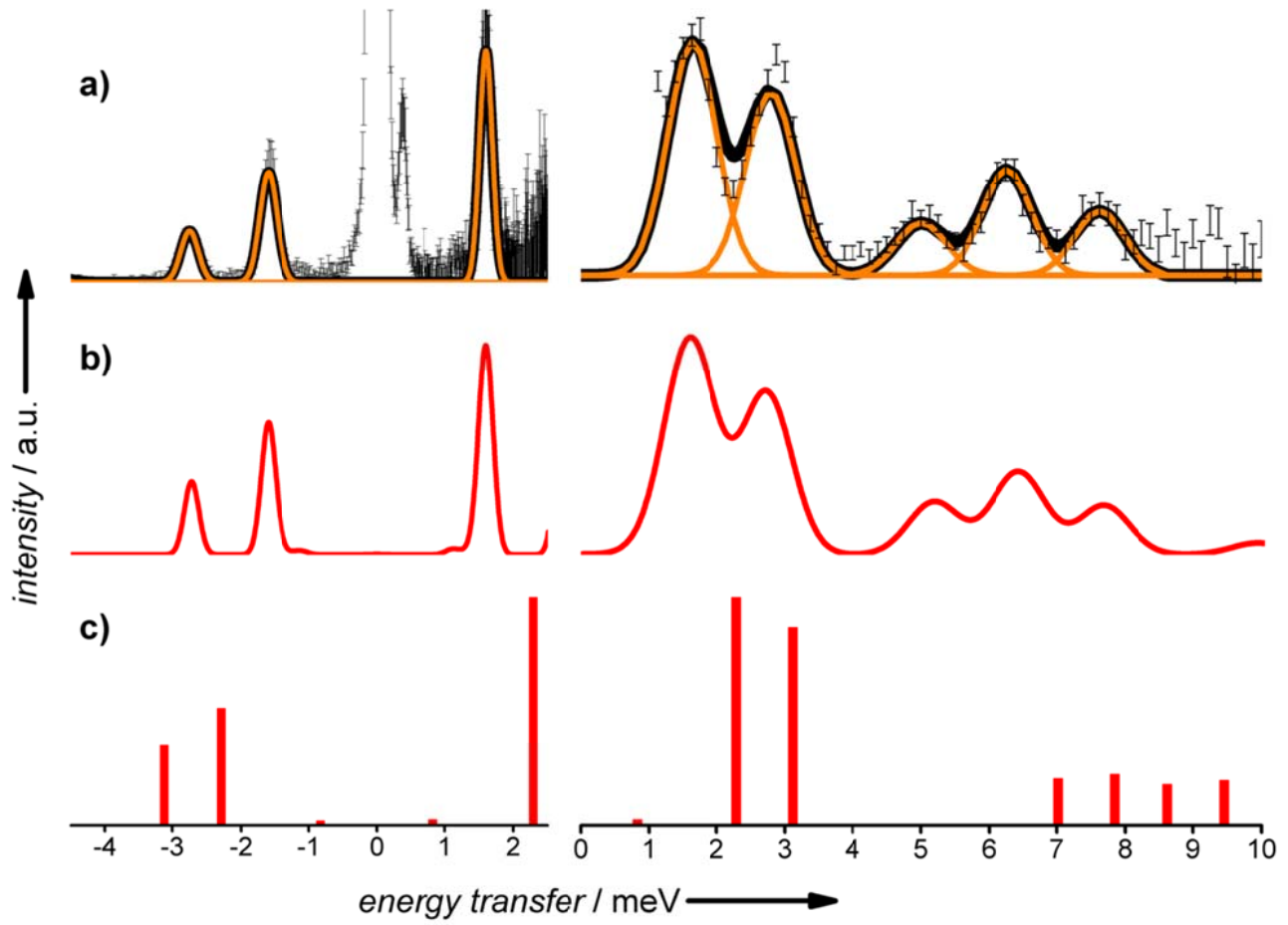
(a)	<b>Tb-a</b>			<b>Tb-b</b>		
O1	0.05225	-0.00323	7.11921	-0.19205	0.22269	-7.15046
O2	-1.25378	-1.33731	4.94483	1.06981	-1.23404	-5.09732
O3	-1.31545	1.30006	4.97095	1.256	1.39347	-5.00111
O4	1.32407	1.36924	4.95861	-1.34821	1.59979	-4.90387
O5	1.37649	-1.24149	4.92996	-1.58306	-1.01093	-5.00122
O6	0.04279	0.03474	3.12176	-0.09014	0.11791	-3.15935
O7	0.09006	-2.69385	3.11583	-0.30837	-2.54682	-3.25163
O8	-2.74217	-2.98706	3.10081	2.52561	-2.94153	-3.36041
O9	-2.63549	-0.0535	3.11431	2.5692	-0.10461	-3.26238
O10	-2.88419	2.78646	3.17968	2.99797	2.72191	-3.23684
O11	-0.03014	2.69736	3.14388	0.13227	2.80004	-3.08621
O12	2.79737	2.98367	3.09654	-2.66838	3.2308	-2.97012
O13	2.72311	0.09527	3.11903	-2.76627	0.33964	-3.0483
O14	2.96279	-2.74072	3.16752	-3.18033	-2.44946	-3.20784
O15	-1.39436	-1.4569	1.20204	1.29423	-1.48625	-1.35655
O16	-1.4372	1.43242	1.22415	1.51685	1.38702	-1.28229
O17	1.41136	1.47444	1.23743	-1.34984	1.58143	-1.18948
O18	1.50674	-1.39784	1.22648	-1.59521	-1.30612	-1.24353
O19	-0.00723	-2.04887	-1.25432	-0.00229	-2.05105	1.24491
O20	-2.00795	0.04105	-1.30679	2.05433	0.00107	1.23307
O21	0.05321	2.02274	-1.29618	0.02335	2.02333	1.23598
O22	2.05043	-0.05016	-1.239	-2.01944	0.00102	1.25773
O23	1.92637	-1.91653	-3.11626	-1.89083	-1.90886	3.15993
O24	-0.01698	-4.03044	-3.19739	0.04597	-4.0496	3.19042
O25	-1.87081	-1.8931	-3.20499	1.89525	-1.88564	3.13251
O26	-3.98366	0.05173	-3.28715	4.07155	-0.01534	3.16017
O27	-1.81261	1.92981	-3.22407	1.90461	1.90187	3.13061
O28	0.186	4.01348	-3.22855	-0.01768	4.05659	3.12996
O29	1.99695	1.8498	-3.13394	-1.90136	1.90581	3.12309
O30	4.12138	-0.10669	-3.08398	-4.04427	0.00851	3.14351
O31	0.06822	-0.02724	-3.1751	0.00606	-0.00284	3.14174
O32	0.0833	-1.89885	-5.01044	-6.10E-04	-1.86092	4.97603
O33	-1.76193	-0.0018	-5.05765	1.8935	0.01191	4.97375
O34	0.13273	1.80848	-5.02556	0.01753	1.89089	4.9615
O35	1.97844	-0.0645	-4.98087	-1.84995	-7.50E-04	4.96893
O36	0.15790	-0.05362	-7.17573	-0.00336	0.01093	7.10625
W1	0.00000	0.00000	5.3853	-0.15607	0.19455	-5.42122
W2	-1.58409	-1.69341	2.98583	1.40019	-1.65202	-3.13661
W3	-1.62991	1.61169	2.98991	1.68984	1.59866	-3.04521
W4	1.61709	1.69769	2.99304	-1.5674	1.88468	-2.93104
W5	1.69358	-1.57449	3.00088	-1.84933	-1.37053	-3.00649
W6	0.00352	-2.31222	-3.02346	0.0145	-2.31809	3.01526
W7	-2.2591	0.04166	-3.08377	2.32092	0.0124	3.00058
W8	0.08956	2.28963	-3.06131	0.00135	2.31112	3.00158
W9	2.37822	-0.05454	-2.98942	-2.31556	-0.01155	3.02915
W10	0.10732	-0.01888	-5.43697	0.00000	0.00000	5.38813
Tb	0.00000	0.00000	0.00000	0.00000	0.00000	0.00000

(b)	Main magnetic axes of the first excited doublet g-tensor					
	<b>Tb-a</b>			<b>Tb-b</b>		
X	-0.73912	0.67357	-0.00281	-0.84670	-0.53170	0.01985
Y	-0.67354	-0.73912	-0.00705	0.53102	-0.84679	-0.03108
Z	-0.00682	-0.00332	0.99997	0.03334	-0.01578	0.99932



**Fig. S19** Molecular internal reference system (blue) and orientation of the first pseudo doublet g-tensor axes (red) for **Tb-a** (right) and **Tb-b** (left).



**Fig. S20** Fitted and calculated INS spectra of **Tb-a** at  $\lambda = 4.74 \text{ \AA}$  (left) and  $\lambda = 2.37 \text{ \AA}$  (right) at 30 K. a) Experimental data with Gaussian fitting of magnetic signals (orange lines) and convolution of individual peak contributions (black line). b) Simulated INS spectra (red line) using the set of optimised crystal field parameters as described in the main text. c) Theoretical INS transition probabilities as calculated from the *ab initio* model for **Tb-a**.

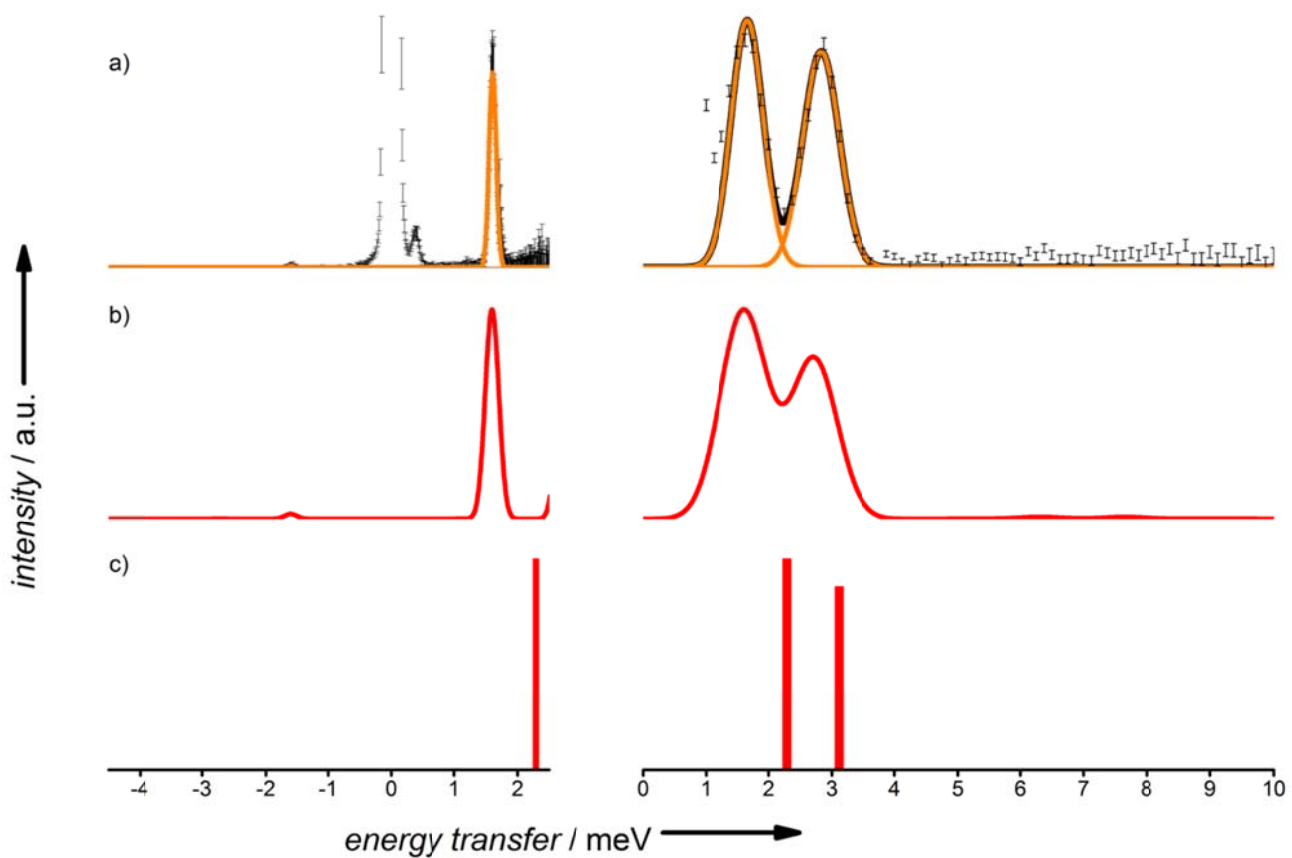


**Fig. S21** Fitted and calculated INS spectra of **Tb-a** at  $\lambda = 4.74 \text{ \AA}$  (left) and  $\lambda = 2.37 \text{ \AA}$  (right) at 5 K. a) Experimental data with Gaussian fitting of magnetic signals (orange) and convolution of individual peak contributions (black). b) Simulated INS spectra (red) using the set of optimised crystal field. c) Theoretical INS transition probabilities as calculated from the *ab initio* model for **Tb-a**.

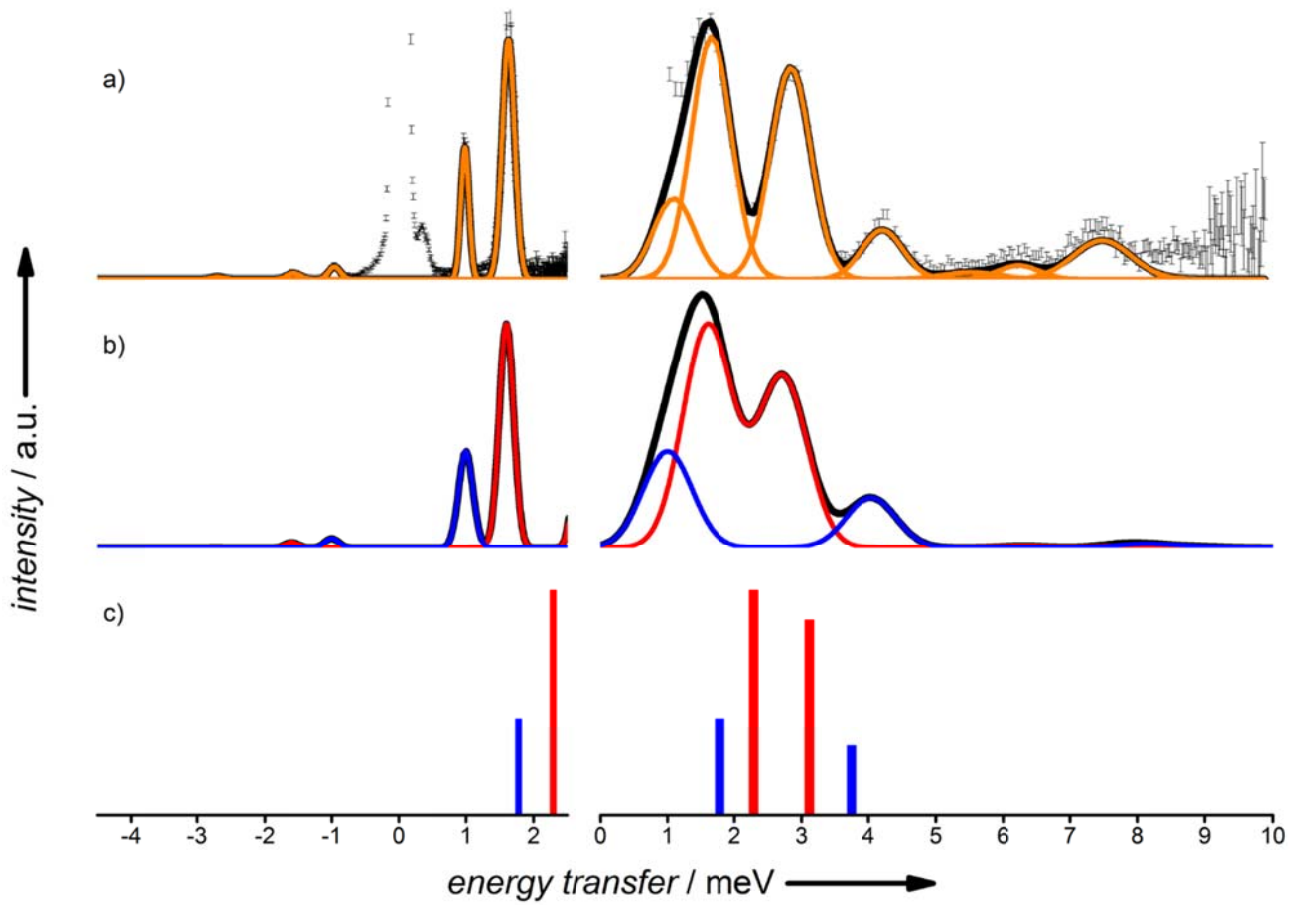


**Fig. S22** Fitted and calculated INS spectra of **Tb** at  $\lambda = 4.74 \text{ \AA}$  (left) and  $\lambda = 2.37 \text{ \AA}$  (right) at 5 K. a) Experimental INS data with Gaussian fitting (orange) and convolution of individual peak contributions (black). b) Simulated INS spectra of **Tb-a** (red) and **Tb-b** (blue) using the set of optimised crystal field and convolution of individual phases contributions (black). c) Theoretical INS transition probabilities as calculated from *ab initio* results for **Tb-a** (red) and **Tb-b** (blue). In all simulations a 70:30 molar ratio of **Tb-a:Tb-b** was assumed.

## References

- 1 R. D. Peacock and T. J. R. Weakley, *J. Chem. Soc. A*, 1971, 1836.
- 2 D. Richard, M. Ferrand and G. J. Kearley, *J. Neutron Res.* 1996, **4**, 33.
- 3 "LAMP, the Large Array Manipulation Program", [http://www.ill.eu/data\\_treat/lamp/the-lamp-book/](http://www.ill.eu/data_treat/lamp/the-lamp-book/)
- 4 (a) C. Rudowicz, C. Y. Chung, *J. Phys. Cond. Matt.* 2004, **16**, 5825; (b) C. Rudowicz, *Coord. Chem. Rev.* 2015, **287**, 28; (c) C. Rudowicz, C. Y. Chung, *J. Phys. Cond. Matter*, 2004, **16**, 5825.
- 5 M. Rotter and A. T. Boothroyd, *Phys. Rev. B* 2009, **79**, 140405.
- 6 S. Kirkpatrick, C. D. Gelatt and M. P. Vecchi, *Science* 1983, **220**, 671.
- 7 F. Aquilante, L. De Vico, N. Ferré, G. Ghigo, P.-A. Malmqvist, P. Neogrády, T. B. Pedersen, M. Pitonák, M. Reiher, B. O. Roos, L. Serrano-Andrés, M. Urban, V. Veryazov and R. Lindh, *J. Comput. Chem.* 2010, **31**, 224.
- 8 V. Veryazov, P.-O. Widmark, L. Serrano-Andres, R. Lindh and B. O. Roos, *Int. J. Quantum Chem.* 2004, **100**, 626.
- 9 G. Karlström, R. Lindh, P.-Å. Malmqvist, B. O. Roos, U. Ryde, V. Veryazov, P.-O. Widmark and M. Cossi, B. Schimmelpfennig, P. Neogradý, L. Seijo, *Comput. Mater. Sci.* 2003, **28**, 222.
- 10 U. Wahlgren, in *Lecture Notes in Quantum Chemistry* (Ed.: B.O. Roos), Springer Berlin Heidelberg, Berlin, Heidelberg, 1992, pp 413-21
- 11 L. Seijo and Z. Barandiarán, in *Computational Chemistry: Reviews of Current* (Ed.: J. Leszczynski), World Scientific, Singapur, 1999, pp 55-152
- 12 B. O. Roos, P. R. Taylor and P. E. M. Sigbahn, *Chem. Phys.* 1980, **48**, 157.
- 13 B. O. Roos and P.-A. Malmqvist, *Phys. Chem. Chem. Phys.* 2004, **6**, 2919.
- 14 L. F. Chibotaru and L. Ungur, *J. Chem. Phys.* 2012, **137**, 064112;
- 15 L. Ungur and L. F. Chibotaru, in *Lanthanides and Actinides in Molecular Magnetism*, Eds. R.A. Layfield and M. Murugesu, Wiley-VCH, 2015, pp 153-184.
- 16 J. J. Baldoví, J. M. Clemente-Juan, E. Coronado, Y. Duan, A. Gaita-Ariño and C. Giménez-Saiz, *Inorg. Chem.* 2014, **53**, 9976.
- 17 M. A. AlDamen, S. Cardona-Serra, J. M. Clemente-Juan, E. Coronado, A. Gaita-Ariño, C. Martí-Gastaldo, F. Luis and O. Montero, *Inorg. Chem.* 2009, **48**, 3467.
- 18 M. Llunell, D. Casanova, J. Cirera, J. M. Bofill, P. Alemany, S. Alvarez, M. Pinsky and D. Avnir, SHAPE 2.0, Universitat De Barcelona & The Hebrew University Of Jerusalem, Barcelona, 2003.